CALIBRATION OF THE GE(LI) GAMMA RAY SPECTROMETER

Garo Balian

A THESIS

in

The Department

of

Physics

Presented in Partial Fulfillment of the Requirements

for the Degree of Master of Science in Physics

at Concordia University, Sir George Williams

campus, Montreal, Canada

CALIBRATION OF THE GE(LI) GAMMA RAY SPECTROMETER

Garo Balian

ABSTRACT

^{226}Ra was used to calibrate a gamma ray spectrometry system based on a 30 cc Ge(Li) detector. Computer codes were devised to handle complex peaks on non-linear backgrounds. An improved energy value of 186.14 ± .04 Kev was determined for the ^{222}Rn transition. Intensity of the 76.6 Kev K_{α} x-rays of daughter products was found to be 44.03 ± 2.12 (with respect to 100 for the 609.19 Kev line from ^{214}Bi), thereby extending the range of usefulness of ^{226}Ra as a calibration standard.

ACKNOWLEDGEMENTS

The author would like to thank Dr. A. L. Kipling for his help with the transfer of Data to the PDP-8/L computer.

In addition, the author is indepted to Dr. S. K. Misra who kindly lent his MCA on several occasions.

Most importantly, the author's sincere appreciation goes to Dr. N. W. Eddy for his guidance and constant encouragement. Without his help, especially in programming and in performing the computer plots, the thesis would have had doubtful success.

TABLE OF CONTENTS

LIST OF FIGURES

1. INTRODUCTION

Environmental radiation monitoring requires accurate knowledge of gamma spectra of naturally occuring radionuclides. Among these, ^{226}Ra is a major constituent of background spectrum. Being already widely used as a gamma source in many undergraduate laboratories ^{226}Ra is gaining acceptance as a research laboratory standard.

Moreover, because of our interest in environmental monitoring, we decided to use ^{226}Ra as a calibration source for the Ge(Li) detector.

When studying radium decay some problems were encountered :

(1) The energy of the 186 Kev decay line was not known to enough precision,

(2) The x-ray energies and relative intensities had not yet been reported,

(3) Data for the gamma ray intensities varied according to authors (see Ch. 7)

We thus determined to upgrade ^{226}Ra plus the entire system of calibration with extra sources.

A radium source, in equilibrium with its decay products, emits at least 47 gamma rays of different energies within the range 186 to 2448 Kev. Among the intense transitions, we re-investigated the 186 KeV line using several sources with accurately known gamma ray energies in the same energy range. A computer program performed a least squares fit of the peak positions, yielding a calibration curve which determined the studied transition energy with good precision.

The main purpose of this work is to extend the use of ^{226}Ra as a relative efficiency calibration source down to 76.6 Kev (the average energy of ^{226}Ra K_{α} x-rays), to be able to quantitatively detect x-rays and low energy gamma rays.

Several methods to determine the areas of peaks are described in Ch. 5 . Individual peaks were fitted by SPETTY, a program similar to the existing SPEC used in the nuclear physics laboratory. In order to handle complex peaks other routines had to be formulated. They derive mainly from GAUSS 2, described in Ch. 6 .

With sources of known intensities (IAEA standard sources etc.), one can determine the absolute detector efficiency. The absolute efficiency is the ratio of the total counts in the spectrum peak in time t over the corresponding total disintegrations of the source in time t.

Our method of determining relative intensities has practical advantages over the standard source technique described above - mainly availability, and of course, cost!

Finally a discussion on expected errors is presented in Ch. 7 . This work contributes to establishing the merit of the methods used by us, and conclusions are drawn.

2. PROBABILITY THEORY AND NUCLEAR PARTICLE DETECTION

2.1. Restricted Statement of Problem

Consider an experiment in which only the occurence or nonoccurrence of an event is recorded. Assume that in a counting device for the detection of radioactive disintegration there are exactly N radioactive atoms present in a sample at the start of the counting period and that each has the same probability p of disintegrating and producing a count during the counting interval. Let $q = 1 - p$ denote the probability that the event will fail to occur. If the event occurs at a given trial, it will be called a success, otherwise a failure. N independent trials are made and let n denote the number of successes obtained in the N trials. Then what is the probability P that exactly n counts will be obtained during the counting period.

For the purpose of deriving the desired formula, we first determine the probability of obtaining n consecutive successes followed by N - n consecutive failures. Since the N events are independent, the probability is:

$$\underbrace{p.p...p}_{n}.\underbrace{q.q...q}_{N-n} = p^n q^{N-n} \qquad (2.1)$$

The probability of obtaining precisely n successes and N - n failures in some other order of occurence is the same as in this particular order because the p's and q's are merely rearranged to correspond to the other order. In order to solve the problem, it is therefore necessary to count the number of orders.

The number of orders is the number of permutations possible with N letters of which n are alike (p's) and the remaining N - n are alike (q's). The number of such permutations is equal to:

$$\frac{N!}{n!(N-n)!} \qquad (2.2)$$

Now, the probability that one or the other of a set of mutually exclusive events will occur is the sum of their separate probabilities; consequently it is necessary to add $p^n q^{N-n}$ as many times as there are different orders in which the desired result can occur. Since (2.2) gives the number of such orders, the probability of obtaining n

successes in some order is therefore given by multiplying $p^n q^{N-n}$ by the quantity in (2.2). The resulting probability, which is that of obtaining n successes in N independent trials of an experiment for which p is the probability of success in a single trial, defines what is known as the Binomial or Bernoulli frequency function.

Consequently,

$$P_n = \frac{N!\, p^n (1-p)^{N-n}}{n!\,(N-n)!} \qquad (2.3)$$

p is the product of the separate probabilities that a given atom will disintegrate, times the probability that the given disintegration will be detected in the given time interval. In general either or both of these separate factors may be very small so that p is usually very small. It is of interest to consider some of the properties of the distribution. Since some result must be obtained

$$\sum_0^N P_n \equiv [p + (1-p)]^N \equiv 1 \qquad (2.4)$$

The term P_n is the (n + 1)th term in the above-indicated binomial expansion. The mean value $u = \bar{n}$

$$u \equiv \bar{n} \equiv \sum_0^N n P_n = pN \sum_0^M \frac{p^m (1-p)^{M-m}}{(M-m)!\, m!} = pN$$

where M = N − 1 and m = (n − 1)

Thus

$$u = \bar{n} = Np \qquad (2.5)$$

Similarly $\bar{n^2}$ is of interest

$$\bar{n^2} \equiv \sum_0^N n^2 P_n = \sum_1^N n^2 P_n = Np \sum_0^M (m+1) \frac{p^m (1-p)^{M-m}\, M!}{m!\,(M-m)!}$$

$$\bar{n^2} = Np \sum_0^M (m+1) P'_m = Np\left[\sum_0^M P'_m + \sum_0^M m P'_m\right] = Np[1 + Mp]$$

or

$$\bar{n^2} = Np\,[Np + (1-p)] \qquad (2.6)$$

where P'_m refers to a different total M rather than N

The quantity $u = \bar{n}$ is the mean value for the number of counts expected from the measurement. It is also of interest to determine the amount by which any given measurement may be expected to deviate from the mean value. The quantity σ used to denote this is called the standard deviation and σ^2 the dispersion of the distribution. σ represents the root mean square deviation

$$\sigma^2 = \sum_0^N (n-u)^2 P_n \equiv u^2 \sum_0^N P_n - 2u \sum_0^N n P_n + \sum_0^N n^2 P_n$$

or

$$\sigma^2 \equiv (\bar{n^2} - u^2) \qquad (2.7)$$

from the definition of $\bar{n^2}$ and u. This result is quite general. For the Binomial distribution

$$\sigma^2 = u(1-p)$$

or

$$\sigma = [u(1-p)]^{1/2} \qquad (2.8)$$

This shows that if p is small, the standard deviation is equal to u. Thus if 100 counts are expected on the average, the actual value of a given count has a good chance of differing from this by about ± 10 or 10%, whereas for 10^6 counts the deviation is 0.1%. If p is near unity $\sigma \ll u^{1/2}$. This will happen for counting only when a short-lived radioactive material is counted over several half-lives and with high (~unity) detection efficiency. The significance of the decreased uncertainty from $u^{1/2}$ is that now most of the active atoms originally present are counted and are not just a small sample.

2.2. Poisson Distribution

When p is very small and N is very large and $n \ll N$, (2.3) becomes simplified by the substitutions

$$N(N-1)\ldots(N-n+1) \approx N^n, \quad (1-p)^{N-n} \approx e^{-p(N-n)} \approx e^{-u}$$

and $p^n N^n = u^n$ giving

$$P_n \approx u^n e^{-u}/n! \qquad (2.9)$$

which is known as the Poisson distribution. This distribution is much more general than (2.3) since, as shown below, it may be derived without assuming that p is the same for each atom.

2.3. General Statement of Problem

The derivation of (2.9) may be made very general using the law of large numbers. The original problem required a constant probability p for all atoms. In general, there is a certain probability (which is usually zero) that any given atom in the universe will disintegrate and be detected by producing a count during the measuring interval. If p_i represents the probability that the ith atom in the universe will produce a count during the measuring interval, what is the probability P_n that exactly n counts will be obtained? We assume $p_i \ll 1$ and $n p_i \ll 1$ in general, let

$$u \equiv \sum_i p_i \qquad (2.10)$$

The derivation of the general term P_n may be understood more readily by considering $P_0, P_1, \ldots$ first. The probability that no counts are obtained is the product of the separate probabilities $(1 - p_i)$ that each atom shall give no count.

Thus $P_0 = \prod_i (1-p_i) \approx \prod_i e^{-p_i} = e^{-\sum p_i} = e^{-u}$

The probability P_1 of just one count is obtained by an extension of the reasoning for P_0

$$P_1 = \sum_j \frac{p_j}{(1-p_j)} \prod_i (1-p_i) = e^{-u} \sum \frac{p_j}{(1-p_j)} \approx e^{-u} \sum p_j = u e^{-u}$$

The term p_j above is the probability that the jth atom will give an effect and the term $(1-p_j)^{-1}\prod_i(1-p_i)$ is the probability that all the rest do not. In the sum, each term has the factor $(1-p_j)^{-1}$. Since $p_j \ll 1$ negligible error results from omitting this factor. Similarly the probability P_n is

$$P_n = \frac{1}{n!} \sum_{a_1,\ldots a_n} \left[\frac{p_{a_1}}{(1-p_{a_1})} \cdots \frac{p_{a_n}}{(1-p_{a_n})} \right] \prod_i (1-p_i) \qquad (2.11)$$

where $a_1, a_2, \ldots$ are p independent subscripts similar to i and j above. If $np_i \ll 1$ we can neglect the $(1-p)$ terms, to obtain

$$P_n \doteq P_n(u) = \frac{e^{-u}}{n!} \sum_{a_1} p_{a_1} \sum_{a_2} p_{a_2} \cdots \sum_{a_n} p_{a_n} = p^n \frac{e^{-u}}{n!} \qquad (2.9)$$

The significance of the separate terms in equation (2.9) are now apparent. e^{-u} is the probability that all other atoms do not give a count, $n!$ the arrangement factor, p^n represents the products of the separate $\sum_i p_i$ terms for each of the n chosen atoms. Actually (2.11) should omit the terms in each sum corresponding to the particular atoms selected by the preceding sum terms. For $np_i \ll 1$ this neglects few terms in the infinite sums to give negligible error.

2.4. Properties of Poisson Distribution

Since the Poisson distribution has been shown to apply quite generally to counting problems involving small sampling i.e $p_i \ll 1$ and $np_i \ll 1$; it is of interest to derive some of the properties of this distribution, similar to those of (2.4-2.8) for (2.3).

$$\sum_0^\infty P_n = e^{-u} \sum_0^\infty \frac{u^n}{n!} = e^{-u} e^{+u} = 1 \qquad (2.12)$$

$$\bar{n} = \sum_0^\infty n P_n = e^{-u} \sum_0^\infty n \frac{u^n}{n!} = e^{-u} \sum_1^\infty \frac{u^n}{(n-1)!} = u e^{-u} \sum_0^\infty \frac{u^m}{m!}$$

$$\bar{n} = u \qquad (2.13)$$

$$\overline{n^2} \equiv \sum_0^\infty n^2 P_n = u e^{-u} \sum_0^\infty \frac{(m+1)\, u^m}{m!} = u e^{-u} \left[u \sum_0^\infty \frac{u^s}{s!} + \sum_0^\infty \frac{u^m}{m!} \right]$$

$$\overline{n^2} = u^2 + u \qquad (2.14)$$

using (2.7), we obtain $\sigma^2 = u$ or

$$\sigma = u^{1/2} \qquad (2.15)$$

as for the Binomial distribution when $p \ll 1$.

2.5. Inverse Problem for Counting

The result of the direct problem as given by (2.9), may be written

$$P_n(u) \equiv u^n e^{-u}/n!$$

showing that it is a function both of n the number of counts actually received, and of $u = \sum_i p_i = \bar{n}$, the mean expected number of counts. In practice, when counting, the directly measured quantity is n and the desired quantity is u. The inverse problem may be stated thusly: for an actual count n, what is the probability that the actual value u lies between u and (u + du)? The justification for such a question lies in the assumption that, in principle, the experiment can be repeated as many times as desired to obtain u with any desired accuracy by increasing the total volume of data.

Let f(x) be our frequency function, if one wants the probability that x will assume some value in the interval from x to x + x, it is given by the integral

$$\int_{x_0}^{x_0+\Delta x} f(x)\,dx$$

the mean value theorem of integral calculus may be applied here under the assumption that f(x) is a continuous function to give the value

$$\Delta x\, f(x_0 + \theta\,\Delta x) \qquad 0 < \theta < 1$$

We can now write that (2.9) is also the solution of the inverse problem when written

$$P_n(u)\,du = \frac{u^n e^{-u}}{n!}\,du \qquad (2.16)$$

It should be noted that n is constant and u variable in (2.16) while u was fixed and n variable in (2.9). Also n is variable in integer steps while u is continuously variable. The properties of (2.16) are analyzed:

$$\int_0^\infty P_n(u)\,du = \frac{1}{n!}\int_0^\infty u^n e^{-u}\,du = \frac{n!}{n!} = 1 \qquad (2.17)$$

$\int_0^n x^n e^{-x}\,dx$ is a definition of n! for all values of n (gamma function). This shows exactly unit probability that u has some value.

$$\bar{u} \equiv \int_0^\infty u\,P_n(u)\,du = \frac{1}{n!}\int_0^\infty u^{n+1} e^{-u}\,du = \frac{(n+1)!}{n!} = (n+1) \qquad (2.18)$$

The most probable value u_0 of u is the maximum of (2.16) as seen from the distribution's shape. Hence

$$0 = \frac{d\,P_n(u)}{du} \qquad \text{gives} \qquad u_0 = n \qquad (2.19)$$

This result shows that the most probable value of u is the measured value n. Similarly $\overline{u^2} = \int_0^\infty u^2 P_n(u)\,du = \frac{(n+2)!}{n!}$

$$\overline{u^2} = \bar{u}\,(\bar{u}+1) \qquad (2.20)$$

and $\sigma^2 = \bar{u}$ or $\sigma = (\bar{u})^{1/2}$

$$\sigma = (n+1)^{1/2} \qquad (2.21)$$

This result is similar to (2.15) except that $(n+1)$ is used instead of u. But when $n \gg 1$, the distinction between n and $(n+1)$ is not important.

2.6. Gaussian Distribution

Information concerning the shape of (2.9) is obtained by examining the ratio of the nth term to the preceding term

$$P_n / P_{n-1} = u/n \qquad (2.22)$$

This shows that P_n increases with n for $n<u$ and decreases with n for $n>u$. For $n \gg u$, the terms decrease very rapidly with n since each term is only a small fraction of the preceding one. Similarly, for $n \ll u$, the terms rapidly decrease in size as n is decreased. From (2.22), the maximum occurs for $n = u$; therefore $P_u = P_{u-1}$ are the maximum values. The function P_n has a flat maximum near P_u and drops rapidly on either side. Most of the area of a plot of P_n vs n occurs between $(u-\sigma)$ and $(u+\sigma)$ where $\sigma = u^{1/2}$ from (2.15). The value of P_u is obtained in a convenient form by replacing n! by use of Stirling's formula

$$n! = (2\pi n)^{1/2}\left(\frac{n}{e}\right)^n \qquad (2.23)$$

which already for $n = 10$ differs from n! by less than 0.8%. We obtain using (2.23)

$$P_u = u^u e^{-u}/u! = (2\pi u)^{-1/2} \qquad (2.24)$$

When $u \gg 1$, it is customary to evaluate the probability P_n by assuming that a Gaussian distribution function applies. When suitable approximations are made it is possible to express (2.9) as a Gaussian function as shown below. To do this, we use

$$x \equiv (n-u) \qquad (2.25)$$

as fundamental variable and let $f(x) \equiv P_n$ define $f(x)dx$ = probability for x to lie between x and $(x+dx)$. We assume for convenience, that x is positive.

$$f(x) = P_{u+x} = u^{u+x} e^{-u}/(u+x)! = P_u (u/u+1)\dots(u/u+x)$$

we consider the cases where $|x| \ll u$

$$f(x) = (2\pi u)^{-1/2}\left[(1+1/u)(1+2/u)\dots(1+x/u)\right]^{-1}$$

since $x \ll u$ we may use $(1+\frac{x}{u}) \approx e^{x/u}$ to give

$$f(x) \approx (2\pi u)^{-1/2}\, e^{-\frac{1}{u}(1+2+\dots x)} \approx (2\pi u)^{-1/2}\, e^{-\frac{1}{u}\int_0^x x\,dx}$$

$$f(x) = (2\pi u)^{-1/2}\, e^{-x^2/2u} = (2\pi\sigma^2)^{-1/2}\, e^{-\frac{1}{2}(x/\sigma)^2} \qquad (2.26)$$

This is the commonly-used Gaussian which shows that f(x) decreases rapidly for $|x| > \sigma$. Expressed in terms of standard units $t = x/\sigma$

$$\Phi(t)\,dt = f(x)\,dx = (2\pi)^{-1/2}\, e^{-\frac{t^2}{2}}\,dt \qquad (2.27)$$

The inverse problem with (2.16) as the solution, may also be expressed approximately by a Gaussian distribution when $n \gg 1$ and $|u-n| \ll n$

Let $y \equiv (u-n)$ and $f_n(y)\,dy = \frac{u^n e^{-u}}{n!}\,dy \approx \left(\frac{e}{n}\right)^n \frac{u^n e^{-u}}{(2\pi n)^{1/2}}\,dy = \left(\frac{n+y}{n}\right)^n \frac{e^{-y}\,dy}{(2\pi n)^{1/2}}$

$$\ln\left(\frac{n+y}{n}\right)^n = n\ln\left(1+\frac{y}{n}\right) = n\left[\frac{y}{n} - \frac{1}{2}\left(\frac{y}{n}\right)^2 + \dots\right] \approx y - y^2/2n$$

So $$f_n(y)\,dy \approx (2\pi n)^{-1/2}\, e^{-y+y-y^2/2n}\,dy = (2\pi n)^{-1/2}\, e^{-y^2/2n}\,dy$$

The behavior of $P_n(u)$ is not symmetric in n and u except to the degree that both can be approximately expressed as Gaussian distributions for u and n large and $|u-n| \ll u, n$.

In Fig. 2.1, $P_n(u)$ has been plotted as a function of u for $n = 0, 1, 2, 4, 8, 16$ and in Fig. 2.2 $P_n(u)$ has been plotted as a function of n for $u = 0, 1, 2, 4, 8, 16$. A logarithmic scale is used for the ordinate which should give the curves a parabolic shape if the Gaussian distribution were to apply rigorously. In Fig. 2.3 the Gaussian distribution is plotted in a similar fashion.

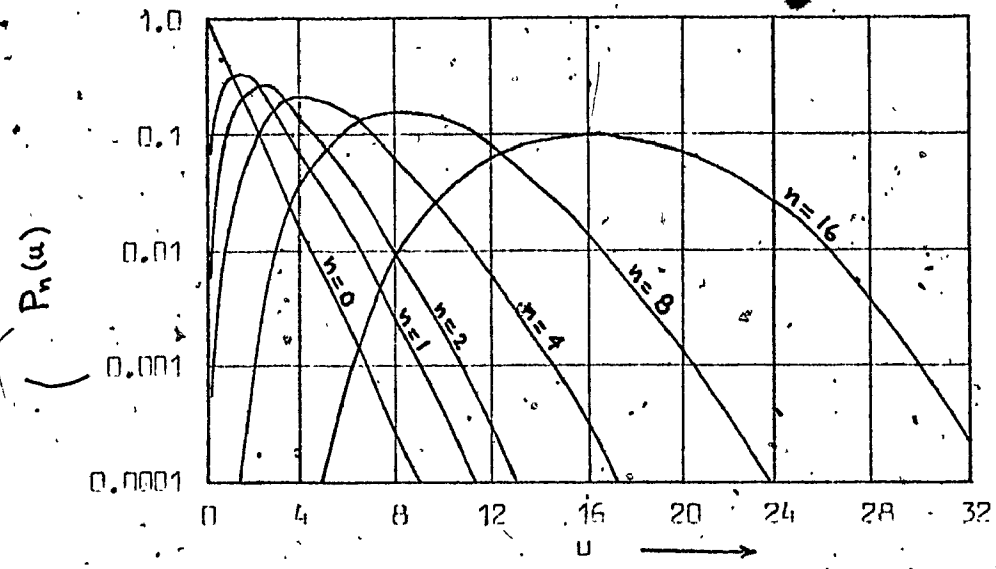

Fig. 2.1

$P_n(u)du$ is the probability that the true mean is between u and $(u + du)$ when n counts are actually obtained.

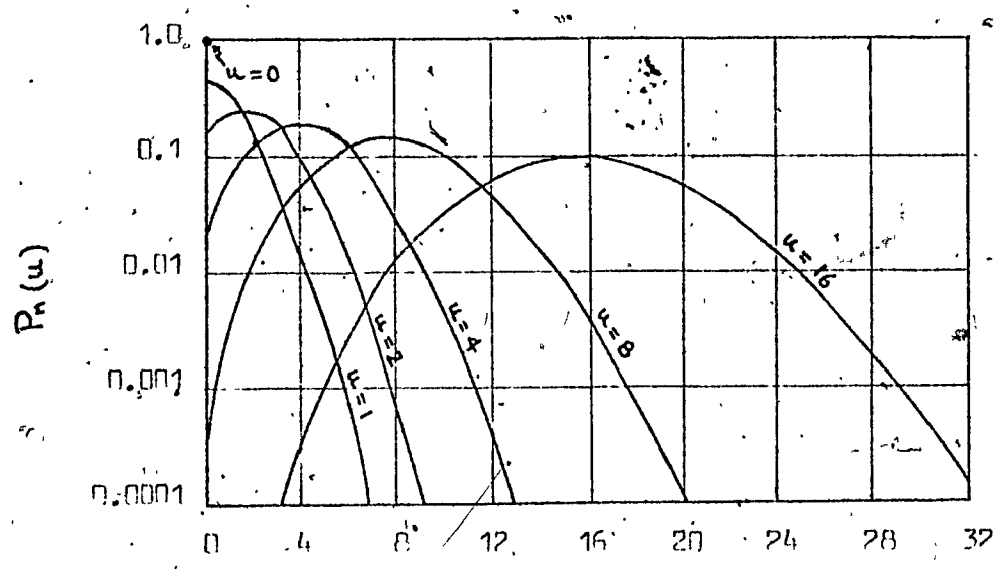

Fig. 2.2

$P_n(u)$ is the probability that exactly n counts will actually be obtained when u is the mean expected result for a count.

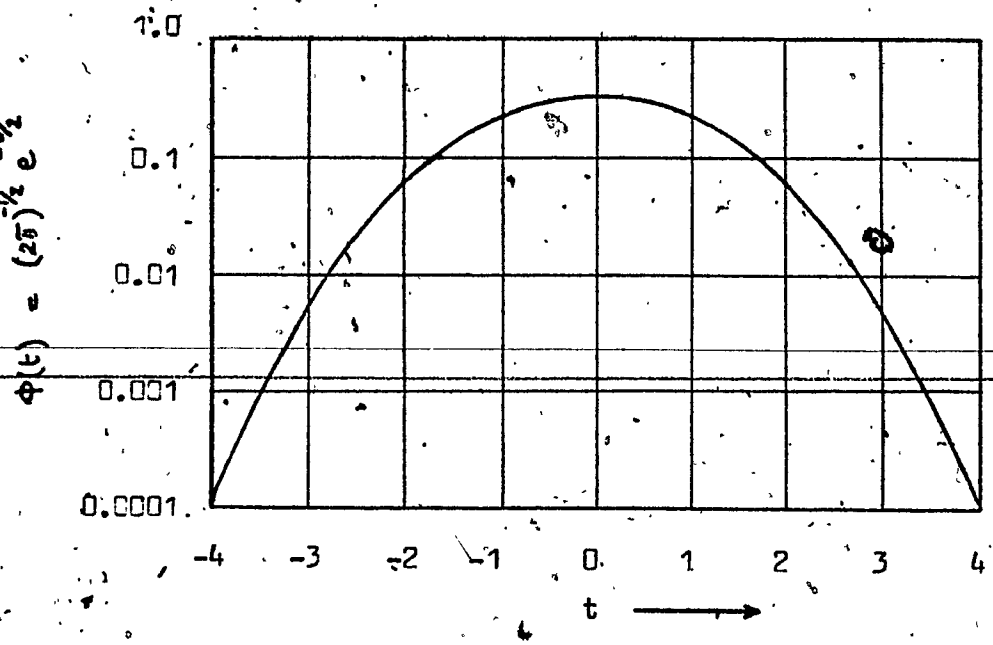

Fig. 2.3

The curve shows the Gaussian function $\phi(t) = (2\pi)^{-\frac{1}{2}} e^{-t^2/2}$ For a large count, this gives the probability that the count will deviate from its mean expected value by t to t + dt times the standard deviation of the count

3. STATISTICAL CHARACTERIZATION OF DATA

The over-all results of a series of n independent measurements $x_1, x_2, \ldots x_n$ of any physical quantity are summarized in the form of a few statistical parameters. These are:

1. The experimenter's estimate of the true value of x, expressed as the mean value $\bar{x}$.
2. The breadth or dispersion found among the individual measurements (expressed as the variance σ^2, or as the standard deviation σ).
3. The extent to which the individual measurements agree with the presumed frequency distribution (expressed as a test of goodness of fit).

3.1. Mean Value

In any finite series of measurements we can never find the exact value of the true mean value m which characterizes the "infinite population" (i.e. an infinite amount) of data. Although the true mean value is constant, our individual measurements are distributed about this mean in a manner given by the particular frequency distribution which describes the process being studied.

The true mean m is that value of x for which the first moment of a frequency distribution is zero. Thus

$$\sum_{x=-\infty}^{x=+\infty} (x-m) P_x = 0$$

defines the mean, where P_x is the probability of the observation x. Geometrically, m is the "center of gravity" of the distribution. The best estimate of m in a finite series of observations is the simple arithmetic average $\bar{x}$ of the n independent measurements, $x_1, x_2, \ldots x_n$

$$\bar{x} = \frac{1}{n} \sum_{i}^{n} x_i \simeq m$$

The "sample mean" $\bar{x}$ approaches the true mean m as number of observations n is increased.

3.2. Variance

The breadth of the statistical distribution of the individual readings about the true mean is expressed by the variance σ^2, or by the square root of the variance which is called the standard deviation σ, of the distribution. For a particular mean m, a small variance σ^2 corresponds to a sharply peaked distribution, whereas a large σ^2 denotes a broad, flattened distribution.

For any frequency distribution, the variance is defined as the average value of the square of the individual deviations (x-m) from the true mean, for an infinitely large number of observations. Thus

$$\sigma^2 \equiv \sum_{x=-\infty}^{x=+\infty} (x-m)^2 P_x \qquad (3.3)$$

or, in terms of a very large series of n independent measurements ($n \gg 1$) of x,

$$\sigma^2 \equiv \frac{1}{n} \sum_{i=1}^{n} (x_i - m)^2 \qquad (3.4)$$

The variance is thus the second moment of the frequency distribution taken about the true mean, m. Geometrically, if a sheet of metal is cut in the shape of the distribution, the variance is the "moment of inertia" of the sheet taken about an axis at x = m and parallel to the frequency axis.

3.3. Sample Variance

In a finite series of n observations we can never determine σ^2 exactly, just as we can never determine m exactly. Our estimate of the true variance σ^2 of the distribution must therefore be based on our imperfect estimate $\bar{x}$ of m. We define accordingly, a sample variance S^2, where m is replaced by $\bar{x}$. Thus the experimental data give

$$S^2 = \frac{1}{n} \sum_{i=1}^{n} (x_i - \bar{x})^2 \qquad (3.5)$$

We introduce briefly the concept of the expected value and some properties. The expected value of a random variable is its mean value

$$E[x] = \sum_{x=0}^{\infty} x f(x)$$

the following properties can be derived ; if c is a constant and g a variable or a function

$$E[cg] = cE[g]$$

$$E[g_1 + g_2] = E[g_1] + E[g_2]$$

We look into the distribution of a sample mean $\bar{x}$ based on a random sample of size n from a population (normal or not).

If x has a frequency function f(x) with mean m and standard deviation σ, let us consider a random sample of size n from this population. The mean of such a sample

$$\bar{x} = \frac{1}{n}(x_1 + x_2 + \dots + x_n)$$

is a random variable because the variables $x_1, x_2, \dots x_n$ corresponding to the n trials of the sample are random variables. Using the properties of E it follows that

$$E[\bar{x}] = E\left[\frac{1}{n}(x_1 + x_2 + \dots + x_n)\right]$$
$$= \frac{1}{n}\sum_{i=1}^{n} E[x_i]$$

But since the sampling is random this implies, by definition, that all the variables have the same frequency function namely that of x, consequently $E[x_i] = E[x] = m$

hence $$E[\bar{x}] = \frac{1}{n}\sum E[x_i] = \frac{1}{n}\sum m$$
$$= m$$

This shows that the mean of $\bar{x}$ is the same as the mean of x, whether x is a normal variable or not. Let us consider

$$n\bar{x} = x_1 + x_2 + \dots + x_n$$

it is the sum of n independent variables all of which have the same frequency function and consequently the same variance σ^2. Knowing that the variance of a sum of independent random variables is equal to the sum of the variance of the variables[1] it follows that

$$\sigma^2_{n\bar{x}} = n\sigma^2 \qquad (3.6)$$

$n\bar{x}$ now being our variable, we rewrite the definition of variance as:

$$\sigma^2_{n\bar{x}} = E[n\bar{x} - E[n\bar{x}]]^2 = E[n^2\bar{x}^2 - 2n\bar{x}E[n\bar{x}] + (E[n\bar{x}])^2]$$
$$= E[n^2\bar{x}^2] - 2n.E[\bar{x}]E[n\bar{x}] + (E[n\bar{x}])^2$$
$$= n^2E[\bar{x}^2] - 2n^2(E[\bar{x}])^2 + n^2(E[\bar{x}])^2$$
$$= n^2\left\{E[\bar{x}^2] - (E[\bar{x}])^2\right\}$$

but the term in brackets is the variance of $\bar{x}$ since

$$\sigma^2_{\bar{x}} = E[\bar{x} - E[\bar{x}]]^2 = E[\bar{x}^2] - 2E[\bar{x}]E[\bar{x}] + (E[\bar{x}])^2$$
$$= E[\bar{x}^2] - (E[\bar{x}])^2$$

thus $$\sigma^2_{n\bar{x}} = n^2\sigma^2_{\bar{x}} \qquad (3.7)$$

Therefore equating (3.6) and (3.7) yields the formula

$$\sigma_{\bar{x}}^2 = \sigma^2/n$$

this is an important result as we shall see next.

Let us consider the expected value of a sample variance S^2, based on a random sample of size n. From the properties of E and the definition of σ^2 it follows that :

$$E[S^2] = E\left[\frac{1}{n}\sum_{i=1}^{n}(x_i-\bar{x})^2\right]$$

now with the help of the substitution : $(x_i-\bar{x}) = (x_i-m)-(\bar{x}-m)$

$$E[S^2] = E\left\{\frac{1}{n}\sum_{i=1}^{n}\left[(x_i-m)-(\bar{x}-m)\right]_i^2\right\}$$

$$= E\left[\frac{1}{n}\sum(x_i-m)^2\right] + E\left[\frac{1}{n}\cdot n(\bar{x}-m)^2\right] - \frac{2}{n}E\left[(\bar{x}-m)\sum(x_i-m)\right]$$

expanding $\sum(x_i-m)$ in the third term :

$$\sum(x_i-m) = \sum x_i - \sum m = n\bar{x} - nm = n(\bar{x}-m)$$

Thus $$E[S^2] = E\left[\frac{1}{n}\sum(x_i-m)^2\right] + E\left[(\bar{x}-m)^2\right] - \frac{2}{n}E\left[n(\bar{x}-m)^2\right]$$

$$= E\left[\frac{1}{n}\sum(x_i-m)^2 - (\bar{x}-m)^2\right]$$

$$= \sigma^2 - \sigma_{\bar{x}}^2 = \sigma^2 - \sigma^2/n$$

$$E[S^2] = \frac{n-1}{n}\sigma^2$$

Then our best estimate of the true variance σ^2 of the distribution in terms of our total finite number n of observations, $x_1, x_2, \ldots x_n$ is

$$\sigma^2 \simeq \frac{n}{n-1}S^2 = \frac{\sum_{i=1}^{n}(x_i-\bar{x})^2}{n-1} \qquad (3.8)$$

3.4. Standard Deviation

The breadth of a distribution of data is best visualized in terms of some statistic which has the same dimension as the mean value. This parameter is the square root of the variance, called the standard deviation σ, of the distribution.

The expected value of the standard deviation corresponds to an infinite population of data. In a finite sample of n independent observations, the best estimate of this standard deviation is to be obtained by evaluating the individual deviations $(x_i-\bar{x})$ from the sample mean $\bar{x}$ and then computing from (3.8) the estimated standard deviation of the parent distribution. This is :

$$\sigma \simeq \left(\frac{1}{n-1}\sum_{i=1}^{n}(x_i-\bar{x})^2\right)^{1/2} \qquad (3.9)$$

But we are interested in uncertainties of the final results, the averages of a finite number n of the readings. From the previous important result: $\sigma_{\bar{x}}^2 = \frac{\sigma^2}{n}$ and using (3.8), our best estimate for the standard error of the mean is

$$\sigma_{\bar{x}} \simeq \left(\frac{1}{n(n-1)} \sum (x_i - \bar{x})^2 \right)^{1/2} \qquad (3.10)$$

3.5. Chi-Squere Test

The most useful statistical test for the "goodness of fit" between data and hypothesis is based on the so-called χ^2 distribution. The χ^2 test may be most simply stated as the quantity:

$$\chi^2 = \sum_{i=1}^{n} \frac{(\text{(observed value)} - \text{(expected value)})^2}{\text{(expected value)}} \qquad (3.11)$$

where the summation is over the total number of independent classification, n, in which the data have been grouped. The observed value also should be subdivided into at least five classifications, each containing at least five events. The expected values are computed from any a priori assumed frequency distribution, i.e. Binomial, Poisson, Gaussian etc... One observes a zero χ^2 for a perfect fit, and in comparing two different fittings the lesser the χ^2 value, the better the fit.

4. THE GAMMA-RAY SPECTRUM

4.1. The Basic Detector

The Ge(Li) detector is typically constructed from a pure single crystal of p type germanium doped with gallium or zinc. The preparation of the loaf (for planar detectors) or the cylinder (for coaxial detectors as in our case), of high resistivity p type germanium is done by the zone refining techniques. Lithium ions are then introduced onto the surface of the germanium bar producing an n type region. These ions are then permitted to drift into the germanium under the influence of a strong electric field. The lithium atoms then compensate or neutralize the p type impurities in the germanium, thus producing intrinsic or compensated material in the drifted region. After the drifting process is completed, there remains a high concentration of lithium atoms at the surface. The intrinsic region, however, becomes the active volume of the detector.

The detector is then reverse biased for the electron-hole collection. This type of drifted detector is referred to as an (n-i-p) device.

4.2. The Basic Interaction

In order to prepare for a discussion of the main features of a complete spectrum, it is necessary to consider in some detail the three principle interactions involved in the detection of gamma radiation. These interactions are :

(a) the photoelectric effect

(b) the Compton effect

(c) pair production

The gammas striking the detector interact by one of these processes, giving kinetic energy to an electron which then loses it in collisions with shell electrons in the germanium lattice. This leaves a trail of electron-hole pairs in the intrinsic region. Since there is an electric field present, these electrons are accelerated to the positive terminal and the holes to the negative terminal. In a good detector, charge collection occurs before significant recombination, and the amount of charge collected at the input of the

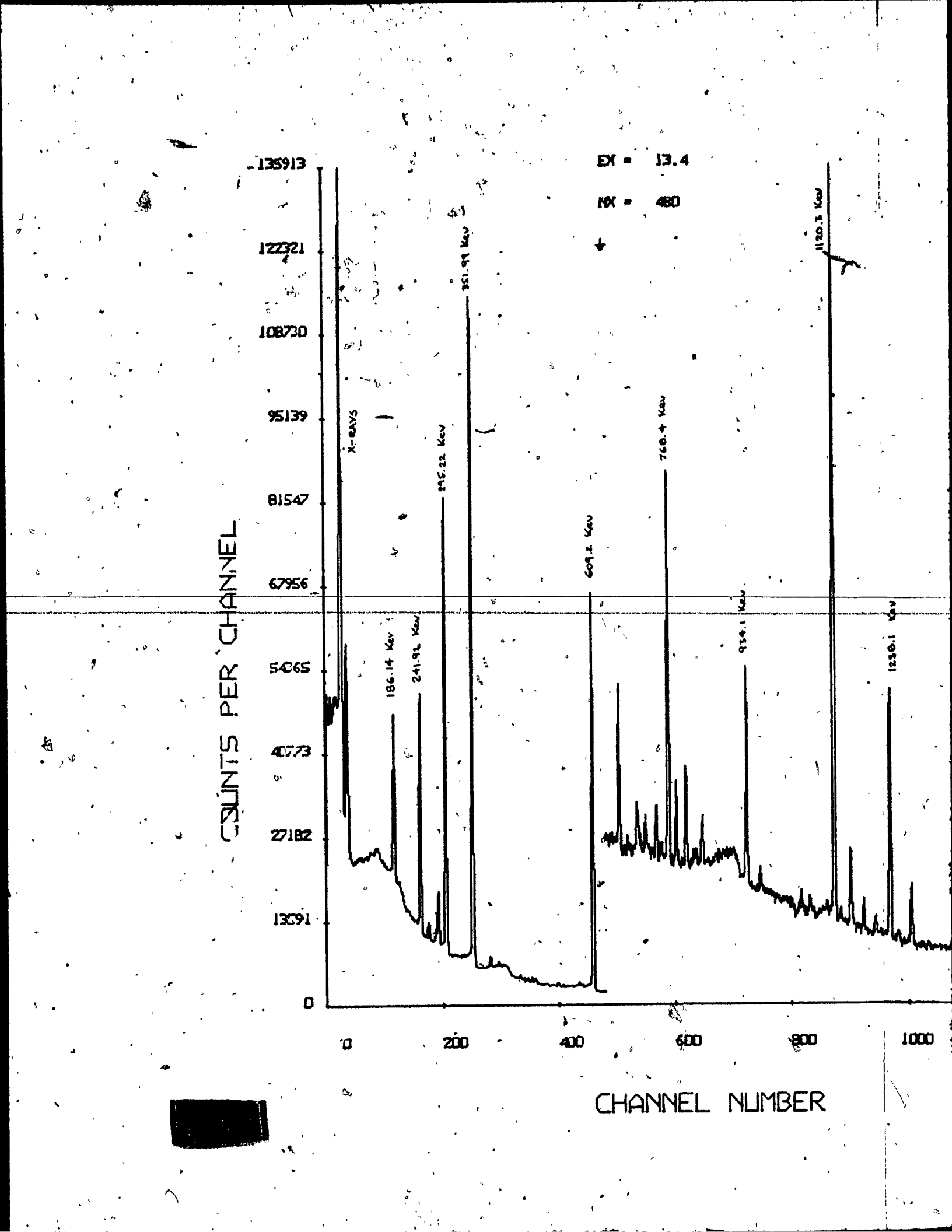
135913
122321
108730
95139
81547
67956
54365
40773
27182
13591
0
COUNTS PER CHANNEL
EX = 13.4
MX = 480
X-RAYS
186.14 Kev
241.92 Kev
295.22 Kev
351.99 Kev
609.2 Kev
768.4 Kev
934.1 Kev
1120.3 Kev
1238.1 Kev
0
200
400
600
800
1000
CHANNEL NUMBER

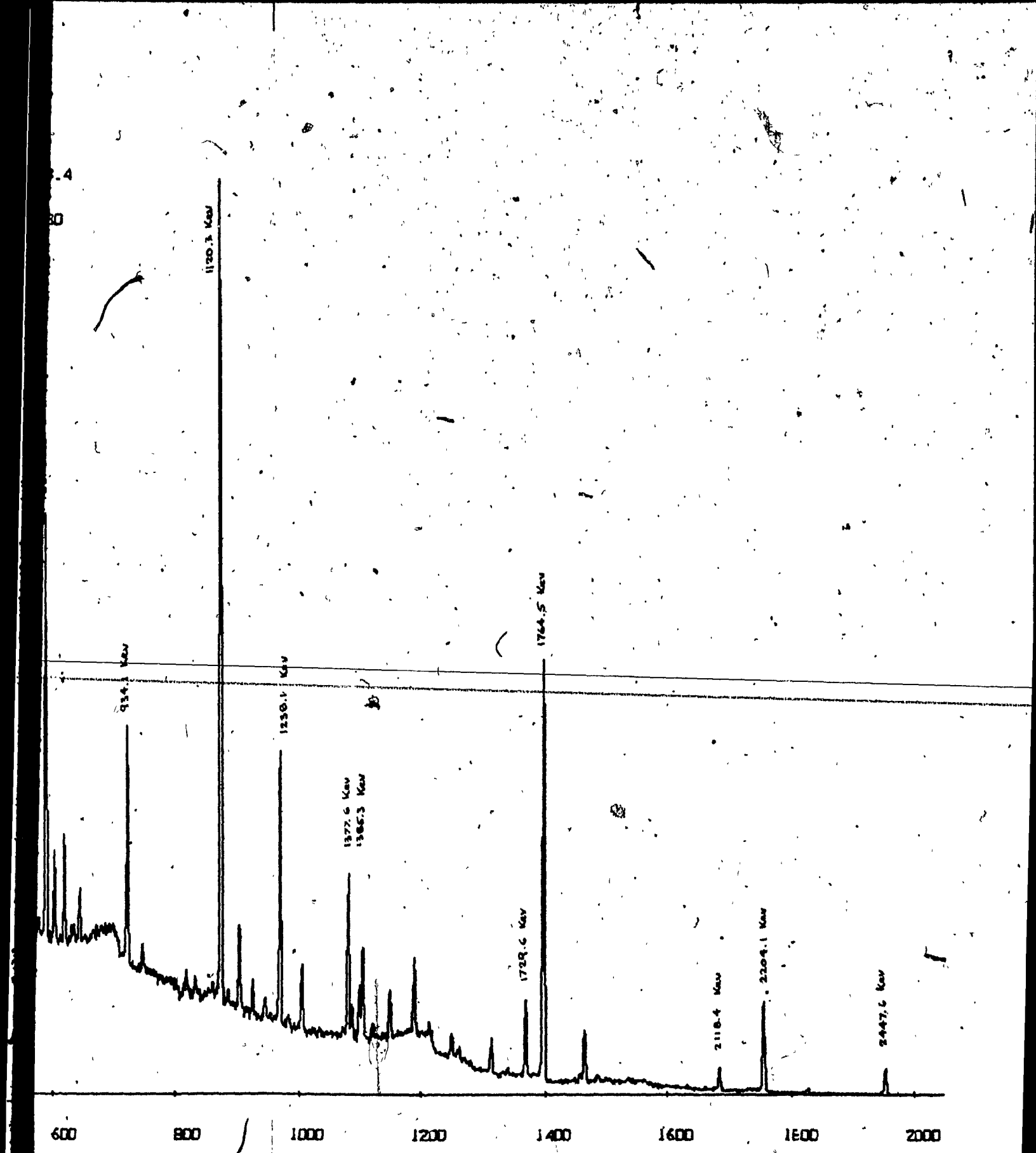
1120.3 Kev
934.1 Kev
1238.1 Kev
1377.6 Kev
1386.3 Kev
1764.5 Kev
1729.6 Kev
2118.4 Kev
2204.1 Kev
2447.2 Kev
600
800
1000
1200
1400
1600
1800
2000

NEL NUMBER

charge sensitive preamplifier is a direct measurement of the number of electron-hole pairs produced. Since this process requires approximately 2.98 ev/electron-hole pair, it is also a direct measurement of the kinetic energy deposited in the intrinsic region by photoelectrons, Compton electrons, positron-electron pairs produced in pair production.

For the photoelectric effect, the energy given the photoelectron is

$$T = h\nu - E_b$$

where T is the kinetic energy of the photoelectron, $h\nu$ the energy of the incoming photon, and E_b is the binding energy of the electron shell from which the photoelectron has come. As the photon energy is increased, the photoelectrons come from deeper and deeper in the atom until the removal of a K electron is most likely. This interaction leaves a vacancy in the K shell, giving rise to characteristic x-ray emission or Auger electrons. Since these latter radiations come within the detector itself, and the photoelectric cross section is very high at these lower energies, this energy is also given to other photoelectrons of lesser energy. The ultimate result is to convert all of the photon energy to the kinetic energy of electrons, which in turn give it up in the formation of electron-hole pairs.

Thus if this were the only process involved, a source of monoenergetic photons such as a gamma-ray source would give a simple sharp line on a pulse-height analyzer, broadened only by statistical considerations. Since the process is governed by the photoelectric cross section, the number of photons undergoing photoelectric interactions and thus becoming a part of the photopeak on a display of count rate vs pulse height decreases approximately as[3]

$$\tau \propto (h\nu)^{-3}$$

where τ is the photoelectric absorption cross section, and $h\nu$ the photon energy.

A second interaction taking place in the crystal is the Compton effect. In this interaction only a portion of the original photon energy is given, in this case, to a loosely bound or "free electron" and a lower-energy photon emerges.

$$h\nu = T + h\nu' \qquad (4.1)$$

where $h\nu$ and $h\nu'$ are the energies of the incoming photon, and scattered photon respectively and T is the kinetic energy given to the electron. Let ϕ and θ be the angles of compton electron and scattered photon with respect to the incoming photon, conservation of momentum gives the following relations

$$h\nu/c = (h\nu'/c)\cos\theta + mv\cos\phi \qquad (4.2)$$

$$(h\nu'/c)\sin\theta = mv\sin\phi \qquad (4.3)$$

(4.1-4.3) can be solved to yield the energy of the scattered photon[4]

$$h\nu' = \frac{h\nu}{1 + h\nu\,(1-\cos\theta)/m_o c^2} \qquad (4.4)$$

where $m_o c^2$ is the rest energy of the electron. But $T = h\nu - h\nu'$ and we obtain the following relation.

$$T = h\nu\left\{1 + [m_o c^2/(1-\cos\theta)h\nu]\right\}^{-1} \qquad (4.5)$$

From (4.4) we see that no minimum kinetic energy exists and that $T \to 0$ as $\theta \to 0$. A maximum does exist, however, at $\theta = 180°$. This is the case of a head-on collision with an electron, with the scattered photon going back at $\theta = 180°$ and the electron going directly forward. This gives

$$T_{max} = h\nu\left[1 + (m_o c^2/2h\nu)\right]^{-1} \qquad (4.6)$$

The theoretical shape of this distribution has been derived by Davisson and Evans[5]. Once the photon energy is given up to electrons in the detector the detection process is identical to the description given in the photoelectric process, except that assuming infinitely good resolution, the pulse height distribution would look like the theoretical distribution shown in Fig. 4.2 .

If we combine the results of the Compton effect with the photoelectric effect, we get the main features of the gamma-ray spectrum from a source with a single gamma energy. In Fig. 4.3 we have a ^{137}Cs spectrum where we note the very pronounced Compton edge at T_{max} = 478 Kev and the approximate correlation between this distribution and the shape of Fig. 4.2 .

As the energy of the photon increases pair production starts and becomes increasingly probable above 1.022 Mev. The initial gamma must have at least this energy because it takes twice .511 Mev to create both positron and electron. In this process the pair is created and

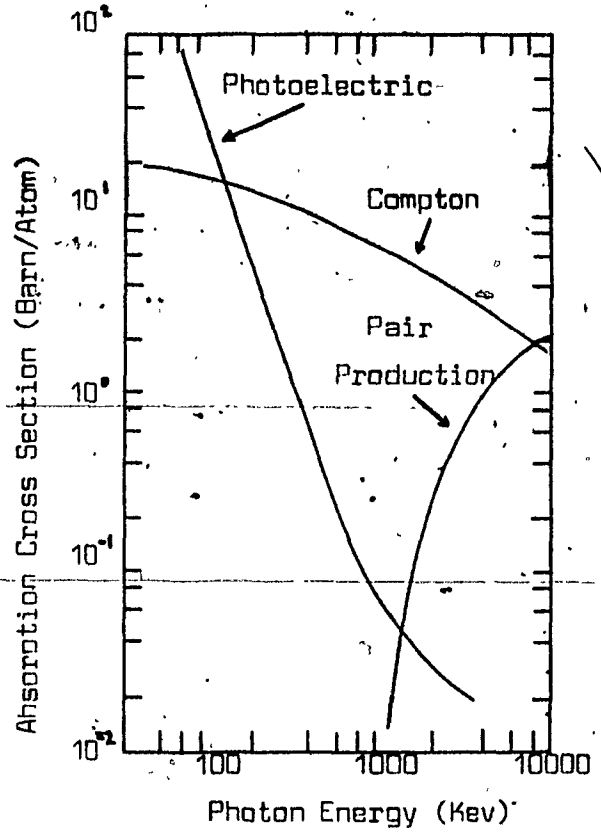

Fig. 4.1

Relative probability of each of the three types of interactions as a function of energy

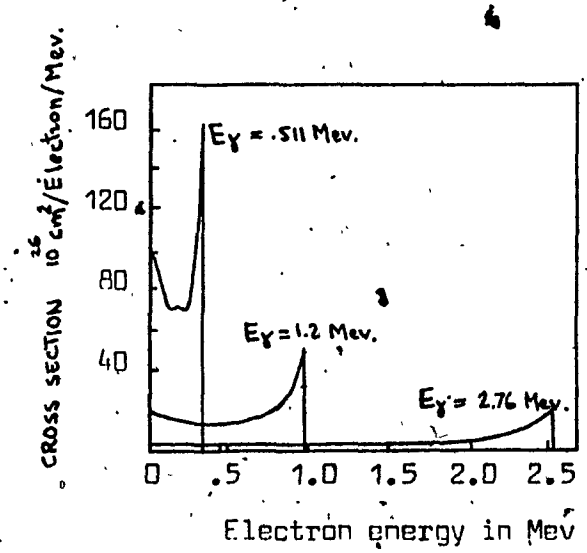

Fig. 4.2

Theoretical Compton distributions, from Davisson and Evans[5]

the kinetic energy of the two members is dissipated in the detector according to the following relation

$$h\nu = 1.022 + T^+ + T^-$$

Since the fate of all positrons is annihilation, as soon as the positron slows down it is captured by an electron and annihilated, typically yielding two .511 Mev photons going in opposite directions to conserve momentum. In a small detector these annihilation photons usually escape the detector without further interaction and the result is that only the kinetic energy T^+ and T^- result in the production of electron-hole pairs and thus a peak (since the process gives rise to a unique energy at $h\nu$ - 1.022 Mev).

In Fig. 4.1 the relative cross sections are shown for photoelectric, Compton and pair production in germanium. The absorption cross section is a measure of the relative probability that an interaction will take place in the detector. It is these probabilities that, for the most part, determine the shape of the observed spectrum. For example, a gamma with an energy of 100 Kev has an absorption cross section of about 55 barns/atom for the photoelectric process and the corresponding Compton cross section is about 18 barns/atom. There is no pair production. This means that at 100 Kev there are three times as many photoelectric interactions as Compton interactions and the sum of counts under the photopeak would be three times the sum under the Compton distribution.

But the shape of a spectrum changes drastically from 100 Kev to 1 Mev . For a gamma of 1 Mev the ratio of Compton cross section to photoelectric cross section is about 90, thus explaining the large Compton distribution at higher gamma energies.

In Fig. 4.4 we summarize various important interactions taking place in a Ge(Li) detector (or in a Sodium Iodide detector, for that matter). We now relate each feature of the spectrum in Fig. 4.5 with one of the interactions shown in Fig. 4.4 .

The two total energy peaks are at 1358.5 and 2753.9 Kev , respectively. For a small detector, the counts under each of these would be owing primarly to interactions of type A . For larger detectors, additional contributions are made by any series of processes which cause all of the gamma energy to be deposited in the crystal.

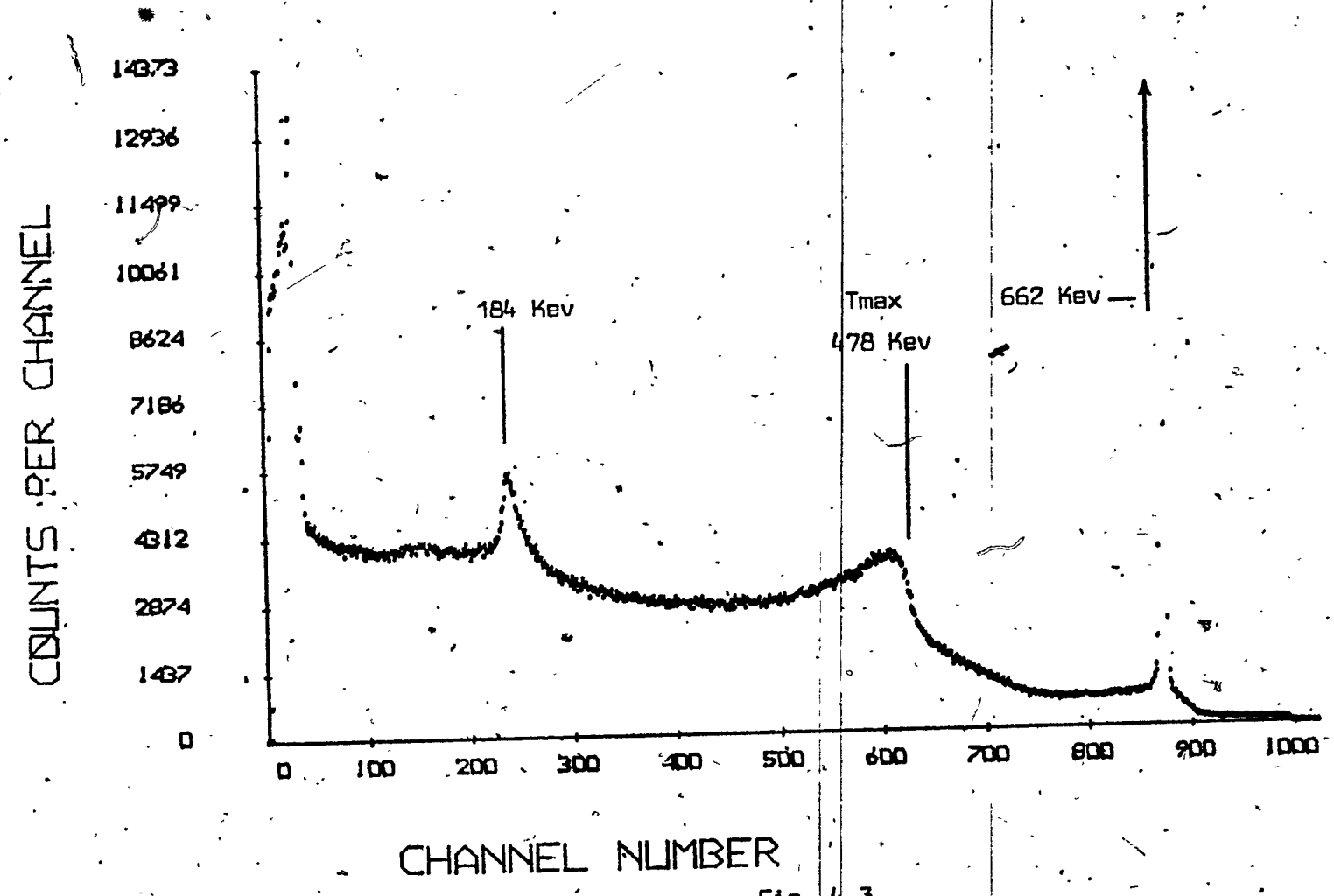

Fig. 4.3

A ^{137}Cs spectrum taken with the Ge(Li) detector. Note the Compton "edge" at 478 Kev, and the backscatter peak at 184 Kev.

Thus interactions of type C become more important as the size of the detector increases.

For a small detector, and for ^{24}Na where there are equal number of gammas of each energy, the ratio of the areas under the two peaks should be the ratios of the photoelectric cross sections.

To the left of each of the total energy peaks, is a Compton edge resulting from interactions of type B . The energy of the "edge" is obtained using (4.6) giving 2520 and 1153 Kev respectively. Two double escape peaks are prominent, and located at 1731 and 346 kev , they correspond to interactions of type D . For small detectors, the ratio of counts under the double escape peaks is the ratio of the pair-production cross sections. In the spectrum, the increase in the pair-production cross section with increasing energy is well shown. Interactions of type E, for single escape, although rare are visible at 2242 Kev . To the left of this peak at 2071 Kev we can barely see the hint of the Compton edge associated with events of type F (i.e the Compton edge of the 2071 Kev peak). The backscatter peak, resulting from events of type G and H is diffuse and located at about 220 Kev . To locate the backscatter peak[6] we recall that a monoenergetic gamma-ray having energy E_γ produces a Compton edge and a backscatter peak in the spectrum at energies

$$E_c = E_\gamma - E_b \qquad (4.7)$$

and

$$E_b = \frac{E_\gamma}{1 + 3.91E_\gamma}$$

where E_γ is expressed in Mev . E_b is nothing else but the minimum value of (4.4) which is a 180° scattered photon. The broadened nature of this peak is the result of more than one gamma-ray energy present in the source and the fact that not all backscatter is at precisely 180°. We also note the presence of a small amount of pair-production in the detector enclosure and environment, or interaction of type I , giving a small peak at 511 Kev .

This is how the quantitative location of the various features of the Ge(Li) detector spectrum gives us an understanding of the basic interaction of the gammas and matter.

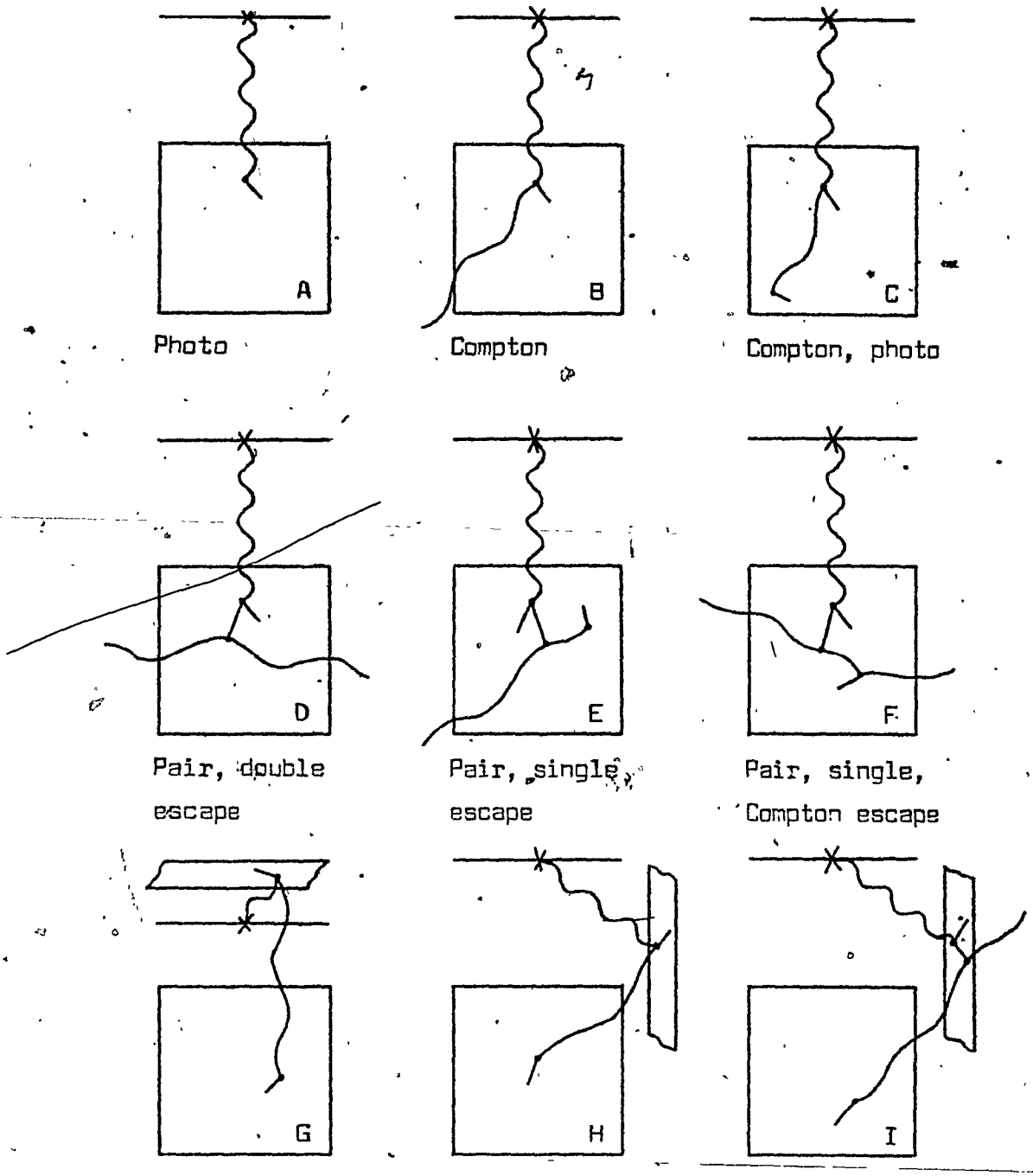

Fig. 4.4

Interaction and combinations of interactions important in interpretation of Ge(Li) detector spectra.

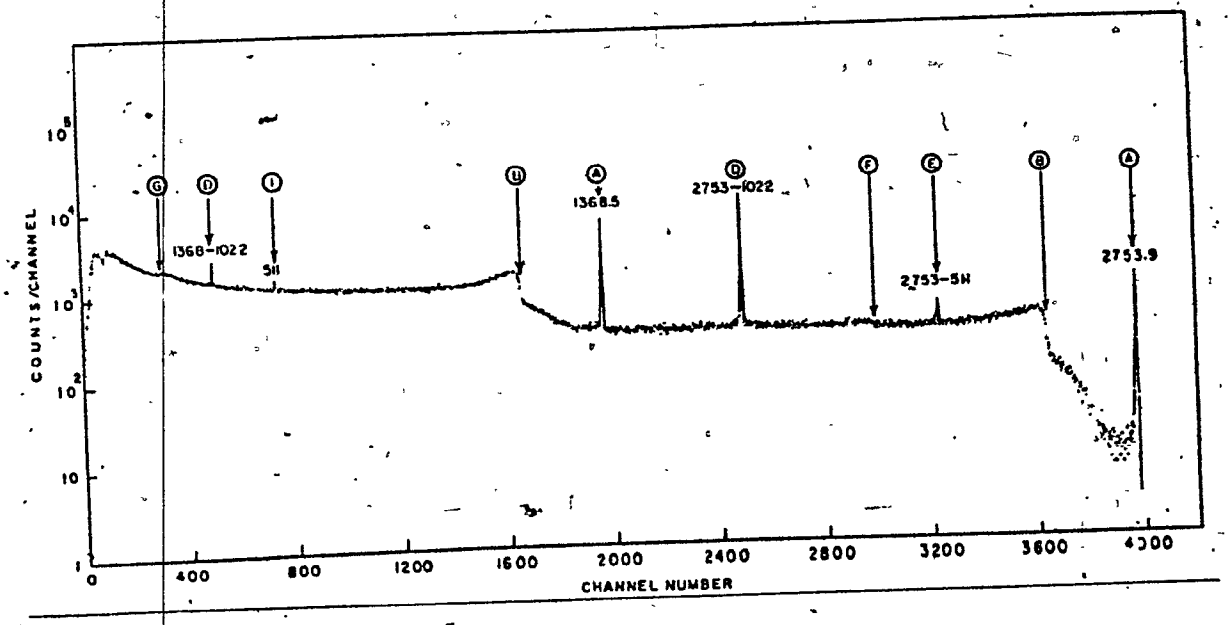

Fig. 4.5

The spectrum of ^{24}Na. There are two gamma rays, 1368.526 and 2753.92 Kev. The letters refer to the type of interactions in Fig. 4.4 which explains that particular portion of the spectrum.

5. FORMULATION OF THE ANALYTIC FUNCTION

In general the basic function used to fit the full energy peak can be written in terms of a Gaussian plus four exponentials. At low energy the width of the Gaussian is determined by the electronic noise of the system. As the energy of the gamma-ray increases, the width becomes larger from statistical processes connected with energy absorption in the detector. And when a cubic background is used, from Fig. 5, we can write the function adopted for a single full energy peak as follows

$$F = a + bx + cx^2 + dx^3 + g\exp(\lambda_1 x) + f\exp(\lambda_2 x) \qquad x_{L1} \leq x \leq x_{L2}$$

$$F = a + bx + cx^2 + dx^3 + h\exp -(x-\mu)^2/2\sigma^2 \qquad x_{L2} < x < x_{R1}$$

$$F = a + bx + cx^2 + dx^3 + K\exp(-\lambda_3 x) \qquad x_{R1} \leq x \leq x_{R2}$$

There are thirteen parameters in the function F : mean of Gaussian μ ; standard deviation σ ; decay length low energy λ_1 ; decay length charge collection λ_2 ; decay length high energy λ_3 ; peak height parameter h ; four background parameters a,b,c,d ; three area parameters f,g,k .

5.1. Background Equation

Some authors[7] use a straight line for the background ; this proves to be a good approximation in the high energy region of the spectrum or where peaks appear to be on a flat background. It is however no longer valid in regions close on a Compton edge or backscatter peak. Furthermore a quadratic background as used by M.Varnell and J.Trischuk[9] was found to be inadequate. We thus turn to a method of baseline construction developed by P.Quittner[6] . Due to the excellent energy resolution of Ge(li) detectors, there are several channels on each side of the peaks of interest which in most practical cases do not contain any other peaks. In these regions a second degree polynomial is fitted to the measured values with least-squares techniques using $2K_L + 1$ and $2K_R + 1$ points around the centres $x_L = x_P - l_L$ and $x_R = x_P + l_R$ respectively, where x_P is the location of the peak (see Fig. 5.2).

The baseline is then constructed in such a way that at x_L and x_R it has the same magnitude (p_L,p_R) and slopes (q_L,q_R) as the fitted

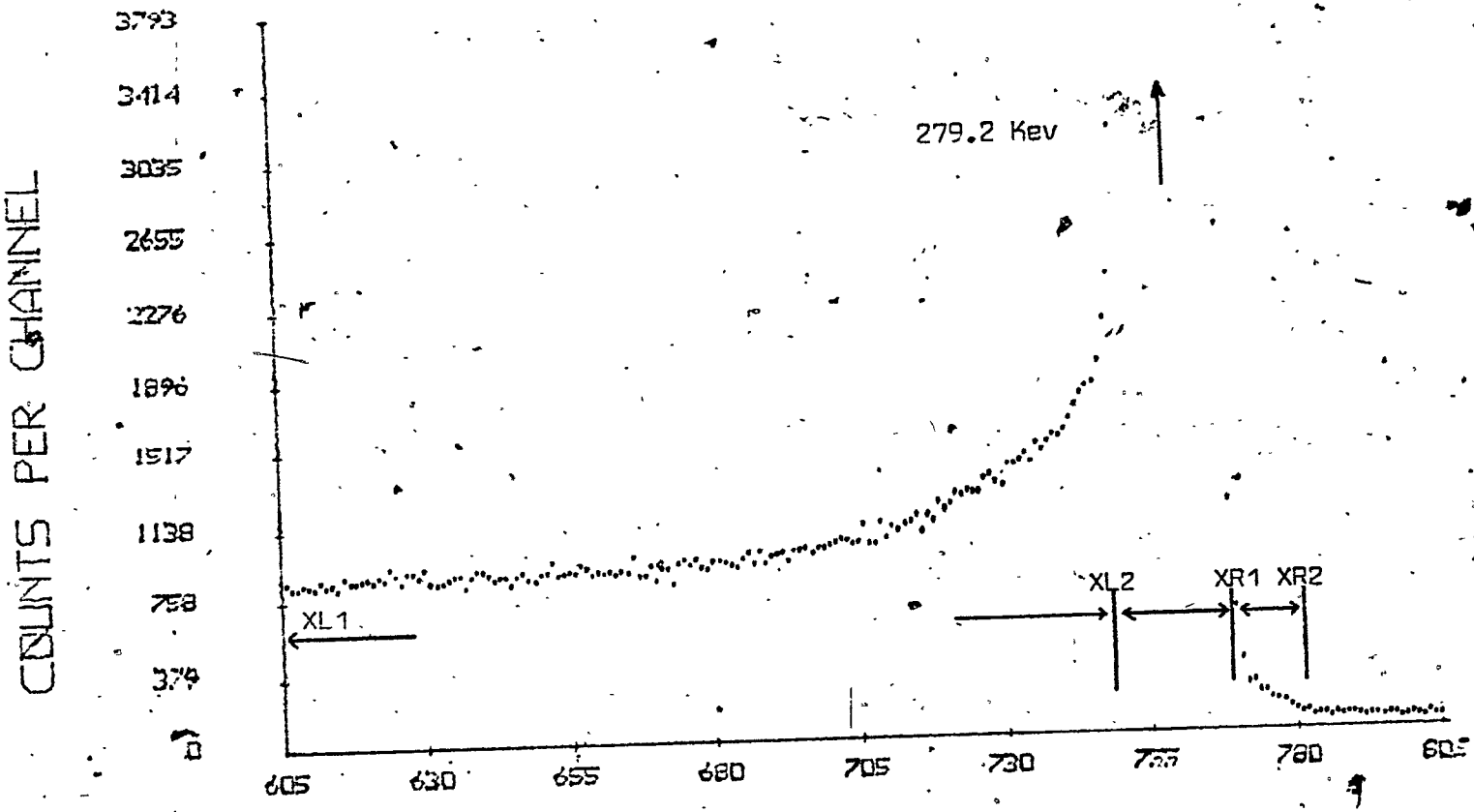

Fig. 5.1

γ-Expanded 279.2 Kev peak of ^{203}Hg, showing exponential tails due to incomplete charge collection and pile up.

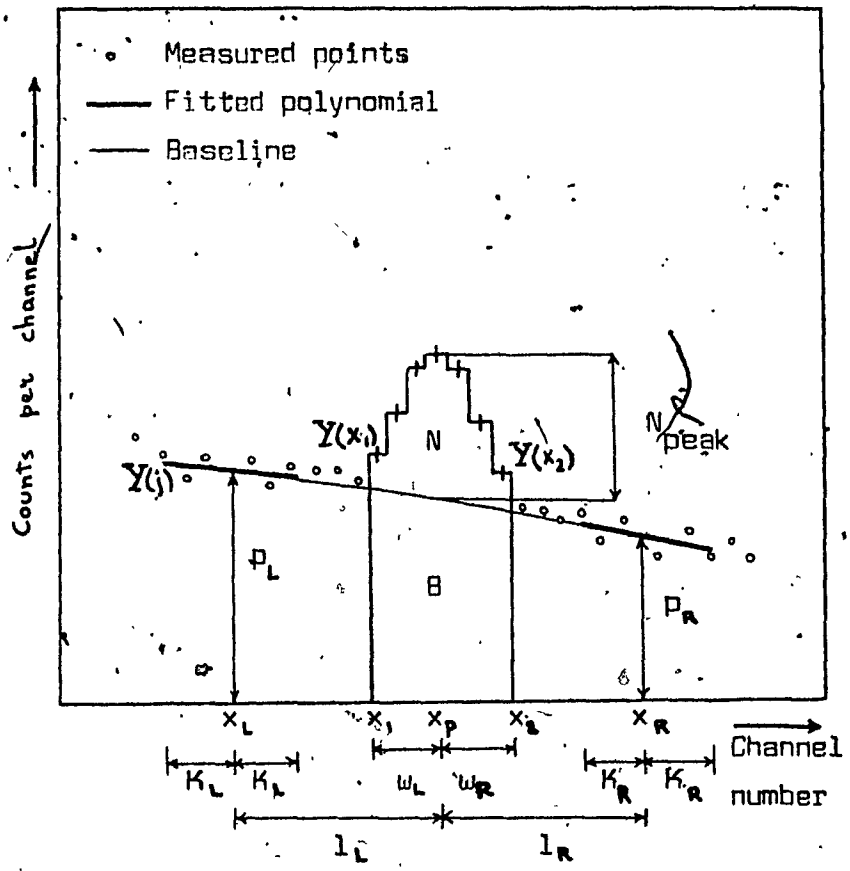

Fig. 5.2

Peak area determination, x_1 and x_2 are the boundaries of the peak region used for peak area calculation, $T = N + B = \sum Y(i)$ = total peak area, B = base area, N = (net) peak area.

polynomials. The simplest polynomial satisfying these conditions is the following cubic :

$$b(x) = p_L + q_L(x - x_L) + \left[\frac{3q_R - 2q_L}{l_L + l_R} + \frac{3(p_R - p_L)}{(l_L + l_R)^2}\right](x - x_L)^2$$

$$+\left[\frac{q_L + q_R}{(l_L + l_R)^2} + \frac{2(p_L - p_R)}{(l_L + l_R)^3}\right](x - x_L)^3$$

The net count in the peak is :

$$N = \sum_{i=x_1}^{x_2} [Y(i) - b(i)] \qquad (5.1)$$

Now the values (p_L, p_R) and the derivatives (q_L, q_R) of the fitting polynomials can be expressed as function of the measured counts (using smoothing constants), for $M = L, R$

$$q_M = 3/[K_M(K_M+1)(2K_M+1)] \sum_{i=-K_M}^{K_M} iY(x_M+i)$$

and for $K_M = 7$.

$$p_M = \frac{1}{1105}\left(\frac{167}{2}Y_0 + 162Y_1 + 147Y_2 + 122Y_3 + 87Y_4 + 42Y_5 - 13Y_6 - 78Y_7\right)$$

for $K_M = 11$

$$p_M = \frac{1}{805}\left(\frac{75}{2}Y_0 + 78Y_1 + 75Y_2 + 70Y_3 + 63Y_4 + 54Y_5 + 43Y_6 + 30Y_7 + 15Y_8 - 2Y_9 - 21Y_{10} - 42Y_{11}\right)$$

where $Y_i = Y(x_M + i) + Y(x_M - i)$, $(i = 0, 1, 2 \ldots 11)$

Peak areas are nearly independent of the fitting regions, provided that :

(a) sufficient points are used to reduce statistical fluctuations i.e. $K_L, K_R \gg 5$

(b) the fitting regions are outside the peak to be determined i.e. $l_L, l_R >$ 3FWHM (FWHM is the full width of the peak at half the maximum height)

(c) the fitting regions do not contain any other peak.

Quittner's method was more successful for fitting single ^{226}Ra peaks on a non linear background than the preceding methods, but failed when required to fit the complex ^{226}Ra peaks at 1378.2 and 1385 Kev .

We could have discarded these two weak intensity peaks from our analysis except for the fact that the ^{226}Ra x-ray peaks also appeared complex in nature. Now since the determination of the areas of these K-line is a major concern of ours in our relative intensity calibration we had to proceed to another method. The next approach that we tried was a simple cubic background which, used with appropriate care in each case, gave good results.

5.2 Exponential Tails.

There are two distinct effects that may give rise to exponential tails : pile-up and incomplete charge collection.

The long tail observed on the low energy side of the Gaussian in Fig. 5.1 , for $XL1 \leq X \leq XL2$, is attributed to incomplete charge collection of hole-electron pairs due to recombination and trapping, this tail is represented by $i \exp(\lambda_2 x)$

Pile up effects occur in the amplifier and are simulated by the low and high energy exponentials; $q \exp(\lambda_1 x)$, $j \exp(-\lambda_3 x)$

These effects, pile up and recombination-trapping occur through the whole spectrum but are of main concern to us in the full energy peak region where they interfere with quantitative measurements of area. At low counting rate, pulse pile up is minimized while for moderate to high counting rate distortions become a problem. In our case we had to make some runs at 35% dead time in order to reduce the time of duration of the runs and achieve spectrum-gain stabilization. The reason for short runs at high counting rates is due to temperature related gain shifts in the ADC electronics, which we tried to compensate for.

Anders[9] has a practical approach to the pulse pile up problem. Pulses from the pulse generator are admixed to the gamma-ray spectrum at a fixed repetition rate. Making two runs, at low and high counting rate it can be demonstrated that the distortion due to pulse pile up will be equivalent for all photopeaks in a spectrum and also equivalent to the distortion of the pulser peak. We can sum the channels which at low counting rate contain the pulser pulses and use this sum, divided by the repetition rate, as measurement of the "pulser time" of the counting interval. At high count rates, the same fraction of timing pulses will be lost from the pulser peak area as are lost from the photopeaks of the gamma-rays.

While this method is appealing, it does not take incomplete charge collection into account which is the predominent effect in our case. We have the following situation : the detector is exposed to radiation and incurs radiation damage in its sensitive region. This damage results in crystal dislocations and defects which constitute traps for liberated charges[9]. These defects are cumulative and

increase the ageing of our six year old detector. The presence of the charge traps reduces the charge collection efficiency of the detector and thus the size of the pulse equivalent to the gamma-ray energy.

Mariscotti[10] and Yule[11] perform respectively second and first derivative smoothing (averaging neighboring points) of the function to fit the peaks. Even so, in their lengthy computer routines provision is not made for the long tail due to incomplete charge collection. Our final approach is similar to that of Donnelly[12] and Quittner[13], and is the following : once we have determined visually peak boundaries, the Gaussian part for χ^2 testing, the exponential forms left and right of the peak, we draw the background and consider (5:1) as giving the net area under the peak.

5.3. Chi-Square Test Discussion

In comparing different fits of the peak, the χ^2 test was used in order to decide which fit is best. When we approximate the ^{226}Ra x-rays by Gaussians and try to handfit the complex peak with a computer program, it has been seen that the classical χ^2 value as in (3.11) depends on heights of the expected or computed values. To minimize fluctuations it was necessary then to remove this dependence and the variance, i.e. the numerator of (3.11) was used instead, as a Figure of Merit for Goodness of Fit. This first approach was successfully applied when dealing with one peak at a time (i.e. when using the same raw data).

For Poisson statistics, we have from (3.11) the conventional test

$$\chi^2 = \sum_{i=1}^{N} \frac{(Y_i - p_i)^2}{p_i}$$

where N = number of channels enclosing the peak. This can be rewritten

$$\chi^2 = \sum \Delta Y_i^2 / p_i \qquad (5.2)$$

where ΔY_i are called residuals.

The relative error e_i per channel is $|\Delta Y_i|/p_i$, and

$$\bar{e}_i = \frac{1}{N} \sum e_i = \frac{1}{N} \sum \frac{\Delta Y_i}{p_i} \qquad (5.3)$$

is the average relative error per peak channel.

If we evaluate (5.2), it has units of xy^2/y, where x = channel no.

and y = counts/channel, or xy = area under the peak ≡ counts. Therefore for two peaks with equally good fits (same relative error per channel e_i), the one with the largest area will give a larger χ^2. In (5.3) however, there are no units thus (5.3) should be independent of area, meaning that if a Gaussian $C \exp -(x-\mu)^2/2\sigma^2$ is considered, $\bar{e}_i$ will be independent of both variations in peak height C or width σ.

But (5.3) is not yet the ideal Figure of Merit for Goodness of Fit because statistical scatter is greater at the tails than at the centroid μ. It is due to the counts/channel being larger at μ than at the tails. Furthermore $e_i = |\Delta Y_i|/p_i$ is greatest at the tails since here $p_i \to 0$. Therefore the major contribution to $\bar{e}_i$ in (5.3) comes from the peak tails where the fit is poorest due to statistical scatter.

We propose the following remedy : in (5.3) we replace the denominator by the average or expected value of p. The single Gaussian function $C \exp -(x-\mu)^2/2\sigma^2$, has first to be normalized in order to yield the frequency function. Replacing $x-\mu$ by x to simplify the integration, we obtain :

$$\int_{-\infty}^{\infty} C \exp -x^2/2\sigma^2 \, dx = 2C\sqrt{2}\,\sigma \int_0^{\infty} \exp -y^2 dy = \sqrt{2\pi}\, C\sigma$$

Hence the normalized Gaussian, or frequency function is

$$g(x) \equiv \left(1/\sqrt{2\pi}\,\sigma\right) \exp -x^2/2\sigma^2$$

From the definition of the expected value, we have

$$\bar{p} = \int_{-\infty}^{\infty} p(x)\, g(x)\, dx = \int_{-\infty}^{\infty} C e^{-x^2/2\sigma^2} \cdot \frac{1}{\sqrt{2\pi}\,\sigma} e^{-x^2/2\sigma^2} dx = \frac{2C}{\sqrt{2\pi}\,\sigma} \int_0^{\infty} e^{-x^2/\sigma^2} dx$$

$$\bar{p} = C/\sqrt{2} \qquad (5.4)$$

For a complex peak formed by two Gaussian functions having the same σ

$$\int_{-\infty}^{\infty} \left[C_1 e^{-(x-\mu_1)^2/2\sigma^2} + C_2 e^{-(x-\mu_2)^2/2\sigma^2} \right] dx = \sqrt{2\pi}\,\sigma\,(C_1 + C_2)$$

Hence, the expected value of p becomes

$$\bar{p} = \int_{-\infty}^{\infty} \left[C_1 e^{-(x-\mu_1)^2/2\sigma^2} + C_2 e^{-(x-\mu_2)^2/2\sigma^2} \right] \left[\frac{C_1 e^{-(x-\mu_1)^2/2\sigma^2}}{\sqrt{2\pi}\,\sigma(C_1+C_2)} + \frac{C_2 e^{-(x-\mu_2)^2/2\sigma^2}}{\sqrt{2\pi}\,\sigma(C_1+C_2)} \right] dx$$

$$\bar{p} = \frac{2}{\sqrt{2\pi}\,\sigma(C_1+C_2)} \left[\int_0^{\infty} C_1^2 e^{-(x-\mu_1)^2/\sigma^2} dx + \int_0^{\infty} C_2^2 e^{-(x-\mu_2)^2/\sigma^2} dx \right] + \frac{4}{\sqrt{2\pi}\,\sigma(C_1+C_2)} \int_0^{\infty} C_1 C_2 e^{-(x-\mu_1)^2/2\sigma^2} e^{-(x-\mu_2)^2/2\sigma^2} dx \qquad (5.5)$$

Considering the term in the third integral

$$e^{-(x-\mu_1)^2/2\sigma^2} \cdot e^{-(x-\mu_2)^2/2\sigma^2} = e^{[-1/2\sigma^2][2x^2-2(\mu_1+\mu_2)x+\mu_1^2+\mu_2^2]}$$

but : $2x^2 - 2(\mu_1+\mu_2)x = \alpha x^2 - \beta x = \alpha(x-\beta/2\alpha) - \beta^2/4\alpha$

$$= 2\left[x - \frac{\mu_1+\mu_2}{2}\right] - \left(\frac{\mu_1+\mu_2}{2}\right)^2$$

let $y = \left[x - \frac{\mu_1+\mu_2}{2}\right]$

we have

$$e^{(-1/2\sigma^2)[2y^2 - \left(\frac{\mu_1+\mu_2}{2}\right)^2 + \mu_1^2+\mu_2^2]} = e^{-(\mu_1-\mu_2)^2/4\sigma^2} \cdot e^{-y^2/\sigma^2}$$

Thus (5.5) becomes

$$\bar{p} = \frac{c_1^2}{\sqrt{2}(c_1+c_2)} + \frac{c_2^2}{\sqrt{2}(c_1+c_2)} + \frac{\sqrt{2}\,c_1c_2}{c_1+c_2} e^{-(\mu_1-\mu_2)^2/4\sigma^2}$$

hence we obtain a dependence only on the difference between the two centroids, and not on their positions .

Our original goal was to formulate GAUSS 2 , the program to fit complex peaks with two Gaussians having the same σ . Since then however, other programs were extrapolated and we have formed : SPETTY which fits a single Gaussian and uses (5.4) as average value of p , GAUSS 6 which deals with two Gaussians having two different σ's and for which the calculation of the value of $\bar{p}$ follows,

$$\int_{-\infty}^{\infty}\left[c_1 e^{-(x-\mu_1)^2/2\sigma_1^2} + c_2 e^{-(x-\mu_2)^2/2\sigma_2^2}\right]dx = \sqrt{2\pi}\,(c_1\sigma_1 + c_2\sigma_2)$$

the average value of p is

$$\bar{p} = 2\int_0^{\infty}\left[c_1 e^{-(x-\mu_1)^2/2\sigma_1^2} + c_2 e^{-(x-\mu_2)^2/2\sigma_2^2}\right] \cdot$$

$$\left[\frac{c_1 e^{-(x-\mu_1)^2/2\sigma_1^2}}{\sqrt{2\pi}\,(c_1\sigma_1+c_2\sigma_2)} + \frac{c_2 e^{-(x-\mu_2)^2/2\sigma_2^2}}{\sqrt{2\pi}\,(c_1\sigma_1+c_2\sigma_2)}\right]dx$$

after some simplification we obtain

$$\bar{p} = \frac{(c_1^2\sigma_1 + c_2^2\sigma_2)}{\sqrt{2}\,(c_1\sigma_1+c_2\sigma_2)} + 2c_1c_2\sigma_1\sigma_2\, e^{-(a/2\sigma_1^2\sigma_2^2)} / [(c_1\sigma_1+c_2\sigma_2)(\sigma_1^2+\sigma_2^2)^{1/2}]$$

where a represents : $\sigma_2^2\mu_1^2 + \sigma_1^2\mu_2^2 - (\mu_1\sigma_1^2 + \mu\,\sigma^2)/(\sigma_1^2+\sigma_2^2)$

Depending on the program, we will use one of the previous p values, to perform a Figure of Merit of Goodness of Fit according to the formula

$$\bar{e}_i = \frac{1}{N\bar{p}} \sum \Delta Y \qquad (5.6)$$

We say now that (5.6) is an effective Figure of Merit.

6. COMPLEX PEAK FITTING PROGRAM GAUSS 2

6.1. Main Program

We summarize the main program by emphasizing the method for fitting data to the basic analytic function (i.e. background subtracted)

$$Y = C\exp-(x-\mu_1)^2/2\sigma^2 + D\exp-(x-\mu_2)^2/2\sigma^2 \qquad (6.1)$$

The following is the general method for fitting data to a non linear function. Let us consider the function

$$Y = f(x, c_1, c_2, \ldots, c_m)$$

where the constants c_i enter non linearly into the functional expression. If the constants c_j were known then it would be possible to form a set of true residuals for each observed Y_i :

$$r_i = f(x_i, c_1, \ldots c_m) - Y_i \qquad i = 1,n \qquad (6.2)$$

Here $f(x_i, x_1, \ldots, x_m)$ is the actual value for a given x_i and Y_i is the observed value. However, if estimates of the parameters c_j can be obtained by some method, then the computed residuals can be calculated

$$R_i = f(x_i, c_1^\circ, c_2^\circ, \ldots, c_m^\circ) - Y_i \qquad i = 1,n \qquad (6.3)$$

for $n(x_i, Y_i)$ data pairs. The problem is to obtain improved values of the parameters c_j using a differential-correction technique based on least squares. First, we expand the function $f(x_i, c_1, c_2, \ldots, c_m)$ about the c_j , using the following linear Taylor-series expansion

$$f(x, c_1, c_2, \ldots c_m) = f(x, c_1^\circ, c_2^\circ \ldots c_m^\circ) + \frac{\partial f}{\partial c_1}(c_1 - c_1^\circ) + \ldots \frac{\partial f}{\partial c_m}(c_m - c_m^\circ) \qquad (6.4)$$

Now we define

$$\delta c_j \equiv c_j - c_j^\circ \qquad \frac{\partial f_i}{\partial c_j} \equiv \left.\frac{\partial f}{\partial c_j}\right|_{x = x_i \,;\, c_j = c_j^\circ} \qquad (6.5)$$

Subtracting Y_i from both sides of (6.4) and using the definition (6.5)

$$f(x, c_1, c_2 \ldots c_m) - Y_i = f(x, c_1^\circ, c_2^\circ \ldots c_m) - Y_i + \frac{\partial f_i}{\partial c_1}\delta c_1 \ldots + \frac{\partial f_i}{\partial c_m}\delta c_m \qquad (6.6)$$

Combining (6.2), (6.3), (6.6) gives:

$$r_i = R_i + \frac{\partial f_i}{\partial c_1}\delta c_1 + \frac{\partial f_i}{\partial c_2}\delta c_2 \ldots + \frac{\partial f_i}{\partial c_m}\delta c_m \qquad (6.7)$$

Now we want to minimize the sum of the squares of the residuals r_i

$$Q \equiv \sum_{i=1}^{n} r_i^2 = \sum_{i=1}^{n}\left[R_i + \frac{\partial f_i}{\partial c_1}\delta c_1 + \frac{\partial f_i}{\partial c_2}\delta c_2 \ldots + \frac{\partial f_i}{\partial c_m}\delta c_m\right]^2 \qquad (6.8)$$

Taking the partial derivative of Q with respect to each δc_j, and setting it equal to zero, we obtain a system of m equations :

$$2\sum_{i=1}^{n}\left[R_i + \frac{\partial f_i}{\partial c_1}\delta c_1 + \cdots \frac{\partial f_i}{\partial c_m}\delta c_m\right]\frac{\partial f_i}{\partial c_1} = 0 \qquad (6.9)$$

$$\vdots$$

$$2\sum_{i=1}^{n}\left[R_i + \frac{\partial f_i}{\partial c_1}\delta c_1 + \cdots \frac{\partial f_i}{\partial c_m}\delta c_m\right]\frac{\partial f_i}{\partial c_m} = 0$$

Rearranging (6.9) gives

$$\sum_{i=1}^{n}\left(\frac{\partial f_i}{\partial c_1}\right)^2\delta c_1 + \sum_{i=1}^{n}\frac{\partial f_i}{\partial c_2}\frac{\partial f_i}{\partial c_1}\delta c_2 + \cdots \sum_{i=1}^{n}\frac{\partial f_i}{\partial c_m}\frac{\partial f_i}{\partial c_1}\delta c_m = -\sum_{i=1}^{n}R_i\frac{\partial f_i}{\partial c_1}$$

$$\vdots \qquad (6.10)$$

$$\sum_{i=1}^{n}\frac{\partial f_i}{\partial c_1}\frac{\partial f_i}{\partial c_m}\delta c_1 + \sum_{i=1}^{n}\frac{\partial f_i}{\partial c_2}\frac{\partial f_i}{\partial c_m}\delta c_2 + \cdots \sum_{i=1}^{n}\left(\frac{\partial f_i}{\partial c_m}\right)^2\delta c_m = -\sum_{i=1}^{n}R_i\frac{\partial f_i}{\partial c_m}$$

These equations (6.10) are linear in the corrections δc_j, and we may therefore deal with the problem from this point onward by the method of least squares[14]. At this point the main program calls the subroutine GSS 2 to solve the m equations in m unknowns. Now, back again in the main program, once the δc_j's have been computed in GSS 2, we test if any δc_j is larger than desired. Since the answer to this question is in our hands, the test fails to be satisfactory and we improve on the solution by repeating the process as an iteration, using the new $c_j' = c_j^0 + \delta c_j$ as our initial value.

In the present case, looking at (6.1) our c_j^0 approximations are on : $C, \mu_1, \sigma, D, \mu_2$. Note that the standard deviation is taken to be the same for both Gaussians. This assumption is based on the following arguments. On previous experiments in bandfitting complex peaks there were no significant differences between the two respective σ's. Also throughout the effort, the goal of maintaining the number of equations to a minimum was considered important. Furthermore note that we are fitting the data to the basic analytic function (6.1) only, and not to the superposition of the Gaussians plus the background (an estimate of the background being done previously by another program). By doing this we have reduced the nine simultaneous equations to five (the background being cubic). Had we not had this preoccupation nothing would have kept us from throwing in two left side and two right side exponentials to each peak ending up with the impractical case of

solving more than twenty equations simultaneously! Thus GAUSS 2 deals with five independent equations whose coefficients a_{ij} and b_i, are formed in the following manner

$$a_{11} = \sum\left(\frac{\partial p}{\partial c}\right)^2 \quad a_{12} = \sum \frac{\partial p}{\partial \sigma}\frac{\partial p}{\partial c} \quad a_{13} = \sum \frac{\partial p}{\partial \mu_1}\frac{\partial p}{\partial c} \quad a_{14} = \sum \frac{\partial p}{\partial D}\frac{\partial p}{\partial c} \quad a_{15} = \sum \frac{\partial p}{\partial \mu_2}\frac{\partial p}{\partial c}$$

$$a_{21} = a_{12} \quad a_{22} = \sum\left(\frac{\partial p}{\partial \sigma}\right)^2 \quad a_{23} = \sum \frac{\partial p}{\partial \mu_1}\frac{\partial p}{\partial \sigma} \quad a_{24} = \sum \frac{\partial p}{\partial D}\frac{\partial p}{\partial \sigma} \quad a_{25} = \sum \frac{\partial p}{\partial \mu_2}\frac{\partial p}{\partial \sigma}$$

$$a_{31} = a_{13} \quad a_{32} = a_{23} \quad a_{33} = \sum\left(\frac{\partial p}{\partial \mu_1}\right)^2 \quad a_{34} = \sum \frac{\partial p}{\partial D}\frac{\partial p}{\partial \mu_1} \quad a_{35} = \sum \frac{\partial p}{\partial \mu_2}\frac{\partial p}{\partial \mu_1}$$

$$a_{41} = a_{14} \quad a_{42} = a_{24} \quad a_{43} = a_{34} \quad a_{44} = \sum\left(\frac{\partial p}{\partial D}\right)^2 \quad a_{45} = \sum \frac{\partial p}{\partial \mu_2}\frac{\partial p}{\partial D}$$

$$a_{51} = a_{15} \quad a_{52} = a_{25} \quad a_{53} = a_{35} \quad a_{54} = a_{45} \quad a_{55} = \sum\left(\frac{\partial p}{\partial \mu_2}\right)^2$$

$$b_1 = -\sum R_i \frac{\partial p}{\partial c}$$

$$b_2 = -\sum R_i \frac{\partial p}{\partial \sigma}$$

$$b_3 = -\sum R_i \frac{\partial p}{\partial \mu_1}$$

$$b_4 = -\sum R_i \frac{\partial p}{\partial D}$$

$$b_5 = -\sum R_i \frac{\partial p}{\partial \mu_2}$$

for clarity we can rearrange the equations to obtain a symmetric matrix form

$$\begin{pmatrix} a_{11} & a_{12} & a_{13} & a_{14} & a_{15} \\ a_{12} & a_{22} & a_{23} & a_{24} & a_{25} \\ a_{13} & a_{23} & a_{33} & a_{34} & a_{35} \\ a_{14} & a_{24} & a_{34} & a_{44} & a_{45} \\ a_{15} & a_{25} & a_{35} & a_{45} & a_{55} \end{pmatrix} \begin{pmatrix} Sc \\ S\sigma \\ S\mu_1 \\ S_D \\ S\mu_2 \end{pmatrix} = \begin{pmatrix} b_1 \\ b_2 \\ b_3 \\ b_4 \\ b_5 \end{pmatrix} \qquad (6.11)$$

6.2. Subroutine GSS 2

The subroutine consists of a program that performs a least squares polynomial curve fit. It is able to fit any polynomial from first to fifth degree. The subroutine is called twice from the main program:

(a) the first entry is to perform a least squares fit in order to obtain the cubic equation of the background

(b) the second entry is to solve five simultaneous linear equations in five unknowns.

We can divide the subroutine in two parts

1. Developing the coefficients and constant terms of the N normal equations.
2. Pivotal condensation, elimination and back substitution.

Part 1.

The formalism for applying the method of least squares is available in any book on numerical analysis[15]. In this case, with a cubic background, the calculations result in four normal equations. These are in general

$$\sum_{I=1}^{4}\left(\sum_{L}^{NUMBER} X_L^{I+J-2}\right) C_I = \sum_{L}^{NUMBER} X_L^{J-1} Y_L \quad \text{FOR } J = 1,\ldots,4$$

where NUMBER =number of data pairs. This can be put in matrix form

$$A \times C = B$$

where the first elements on the left form the coefficients A_{IJ}. C_I are the unknowns, the terms on the right form the constants B_I. Part 1. is best explained in detail by looking at the block diagrams in Fig. 6.1,6.2,6.3 .

Part 2.

In this part we investigate the method devised for the numerical solution of simultaneous linear equations. We either have four simultaneous equations when called from Part 1 or five simultaneous equations when called from the main program. Solutions by determinants are quite cumbersome in our case and we rule out the possibility of using Cramer's Rule which is simple only when the number of equations does not exceed three. Also Cramer's Rule includes a step in which one must divide by a determinant, which often becomes very small, thereby producing a singularity which halts the computer and prevents further execution.

We therefore turn to the simpler and more reliable method of Gauss elimination. The theory for solving N simultaneous linear equations in N unknowns follows :

Let the N unknowns be $x_1, x_2, \ldots, x_N$ and let the equations be

$$a_{11}x_1 + a_{12}x_2 + \cdots + a_{1N}x_N = b_1$$
$$a_{21}x_1 + a_{22}x_2 + \cdots + a_{2N}x_N = b_2$$
$$\cdots\cdots\cdots\cdots\cdots\cdots$$
$$a_{N1}x_1 + a_{N2}x_2 + \cdots + a_{NN}x_N = b_N$$

We assume that the equations have been so ordered that $a_{11} \neq 0$. We define N - 1 multipliers

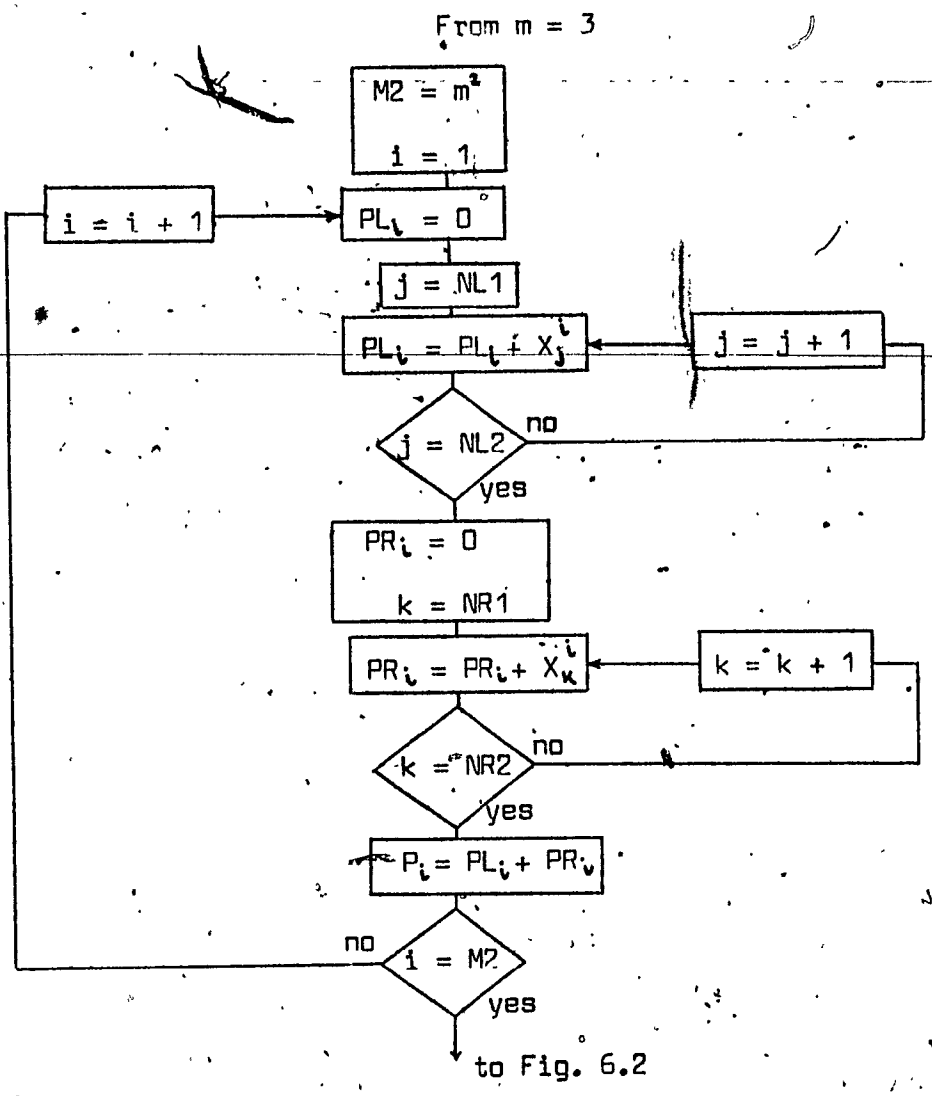

Fig. 6.1

Forming the different powers P_i of X_j. The subscripts j varying from NL1 to NL2 (points taken to the left of curve) and k varying from NR1 to NR2 (points taken to the right of curve).

From Fig. 6.1

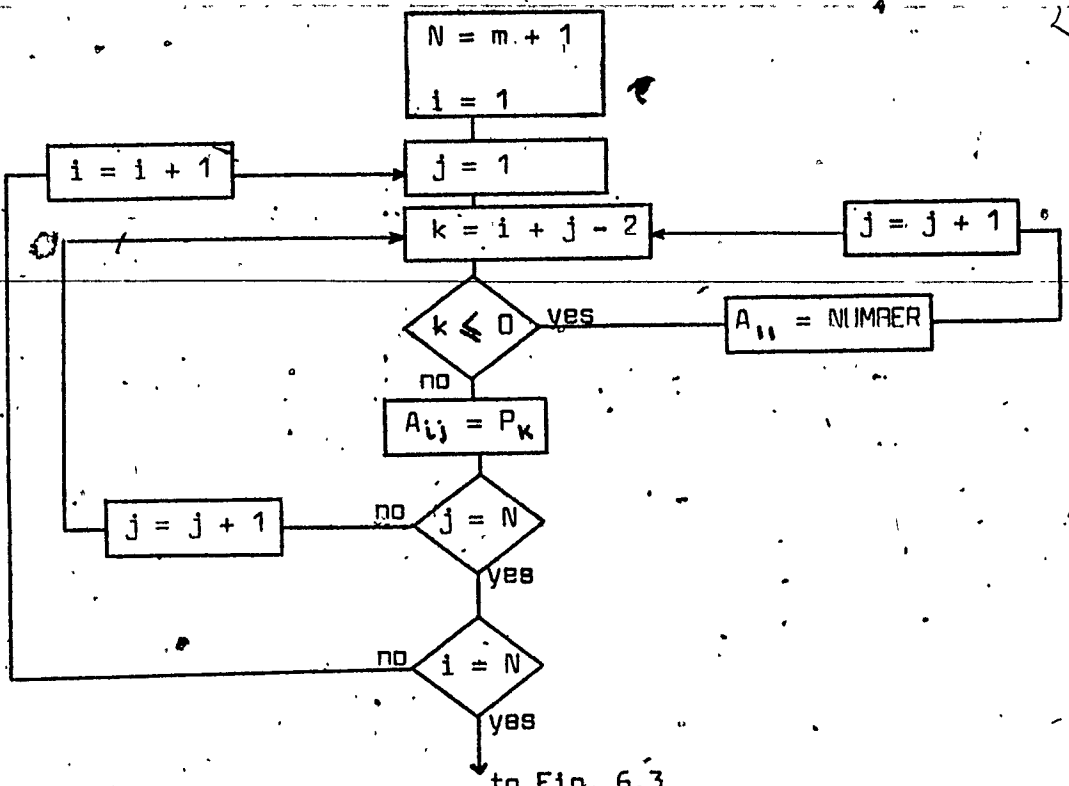

Fig. 6.2

Forming the coefficients of the four equations by assigning the P_i to the matrix elements A_{ij}

From Fig. 6.2

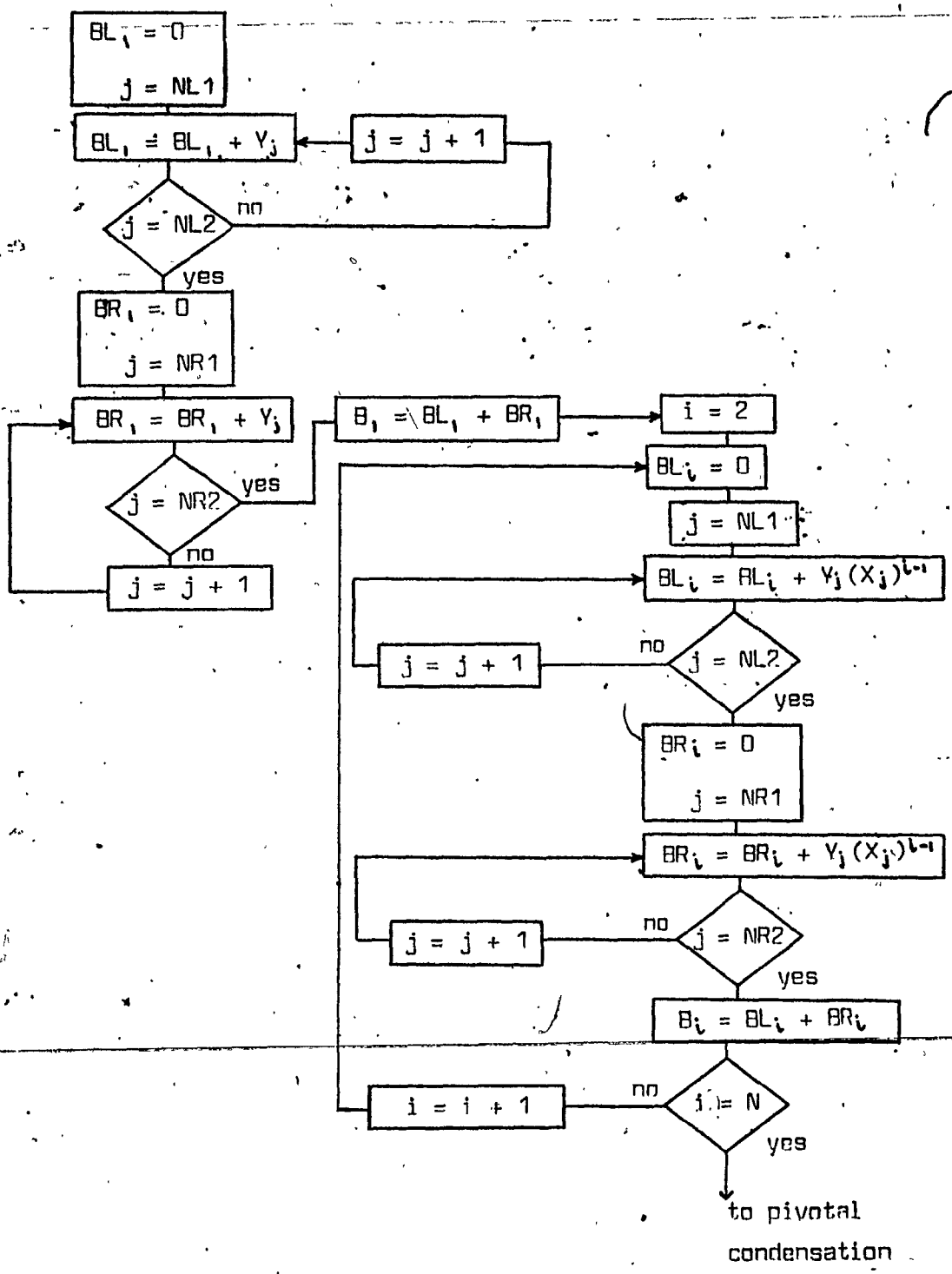

Fig. 6.3

Forming the first constant term B_1, and the following terms B_2, B_3, B_4

$$m_i = a_{i1} / a_{11} \qquad i = 2,3,\ldots,N$$

and subtract m_i times the first equation from the ith equation. If we define

$$a_{ij}' = a_{ij} - m_i a_{1j} \qquad i = 2,\ldots N$$
$$b_i' = b_i - m_i b_1 \qquad j = 1,\ldots N$$

we see that

$$a_{i1}' = 0 \qquad i = 2,\ldots N$$

The transformed equations are

$$a_{11}x_1 + a_{12}x_2 + \ldots + a_{1N}x_N = b_1$$
$$0 + a_{22}'x_2 + \ldots + a_{2N}'x_N = b_2'$$
$$\ldots\ldots\ldots\ldots\ldots\ldots$$
$$0 + a_{N2}'x_2 + \ldots + a_{NN}'x_N = b_N'$$

we continue in this way. At the Kth stage we eliminate x_K by defining multipliers

$$m_i^{(K-1)} = \frac{a_{iK}^{(K-1)}}{a_{KK}^{(K-1)}} \qquad i = K+1,\ldots N \qquad (6.2)$$

where $a_{KK}^{(K-1)} \neq 0$. Then

$$a_{ij}^{(K)} = a_{ij}^{(K-1)} - m_i^{(K-1)} a_{Kj}^{(K-1)}$$
$$b_i^{(K)} = b_i^{(K-1)} - m_i^{(K-1)} b_K^{(K-1)} \qquad (6.3)$$

for $i = K+1,\ldots N$ and for $j = K,\ldots N$

The index K takes on consecutive integer values for 1 through and including $N-1$. At the point where $K = N-1$ we are eliminating x_{N-1} from the last equation.

The final triangular set of equations is given by

$$a_{11}x_1 + a_{12}x_2 + \ldots + a_{1N}x_N = b_1$$
$$a_{22}'x_2 + \ldots + a_{2N}'x_N = b_2' \qquad (6.4)$$
$$\ldots\ldots\ldots$$
$$a_{NN}^{(N-1)}x_N = b_N^{(N-1)}$$

The block diagram for the elimination process is shown in Fig. 6.4, it follows the description fairly closely, with two exceptions. The box marked + containing "arrange rows so that $a_{KK} \neq 0$" refers to a process to be discussed later. As we shall see, possible round off errors in the values of the unknowns can be substantially reduced by a judicious choice of row interchange. The second difference between the block diagram and the description above is that we have used one word, FACTOR, for all multipliers in the block diagram for we never

used more than one multiplier at a time.

In reading the block diagram, note the meanings assigned to the subscripts i, j, K :

K refers to the number of the equation being subtracted from other equations ; it is also the number of the unknown being eliminated from the last N - K equations.

i refers to the number of the equation from which an unknown is currently being eliminated.

j refers to the number of a column.

The back substitution can be described as follows :

$$X_N = b_N^{(N-1)} / a_{NN}^{(N-1)}$$

$$X_{N-1} = \left(b_{N-1}^{(N-2)} - a_{N-1,N}^{(N-2)} X_N \right) / a_{N-1,N-1}^{(N-2)}$$

. . . . . .

$$X_j = \left(b_j^{(j-1)} - a_{jN}^{(j-1)} X_N - \ldots - a_{j,j+1}^{(j-1)} X_{j+1} \right) / a_{jj}^{(j-1)} :$$

for $j = N - 2, \ldots, 1$

The block diagram shown in Fig. 6.5 corresponds to the back substitution.

Now, we recall that we may have to rearrange rows at each stage of the elimination process in order to avoid division by zero. Also it can be seen that at each stage in the process the calculations use the numbers calculated in the previous stage. For large matrices where a considerable number of arithmetic operations is involved, this is the classic situation in which error magnification can take place[16] and we take all the possible steps to minimize the build-up of errors.

From (6.2) and (6.3) we see that one operation which occurs many times is multiplication by m_i. In multiplying the number any accumulated error which is present will also multiplied by m_i ; therefore these multipliers should be made as small as possible, and certainly less than one, so that the errors are not magnified by the multiplication.

This is easily achieved if the pivotal element $|a_{KK}^{(K-1)}|$ is the largest of all the elements $|a_{iK}^{(K-1)}|$ in the same column for $i > K$ in (6.2), then

$$|m_i^{(K-1)}| \leq 1$$

Our rule is then to rearrange the last N - K + 1 rows so that the

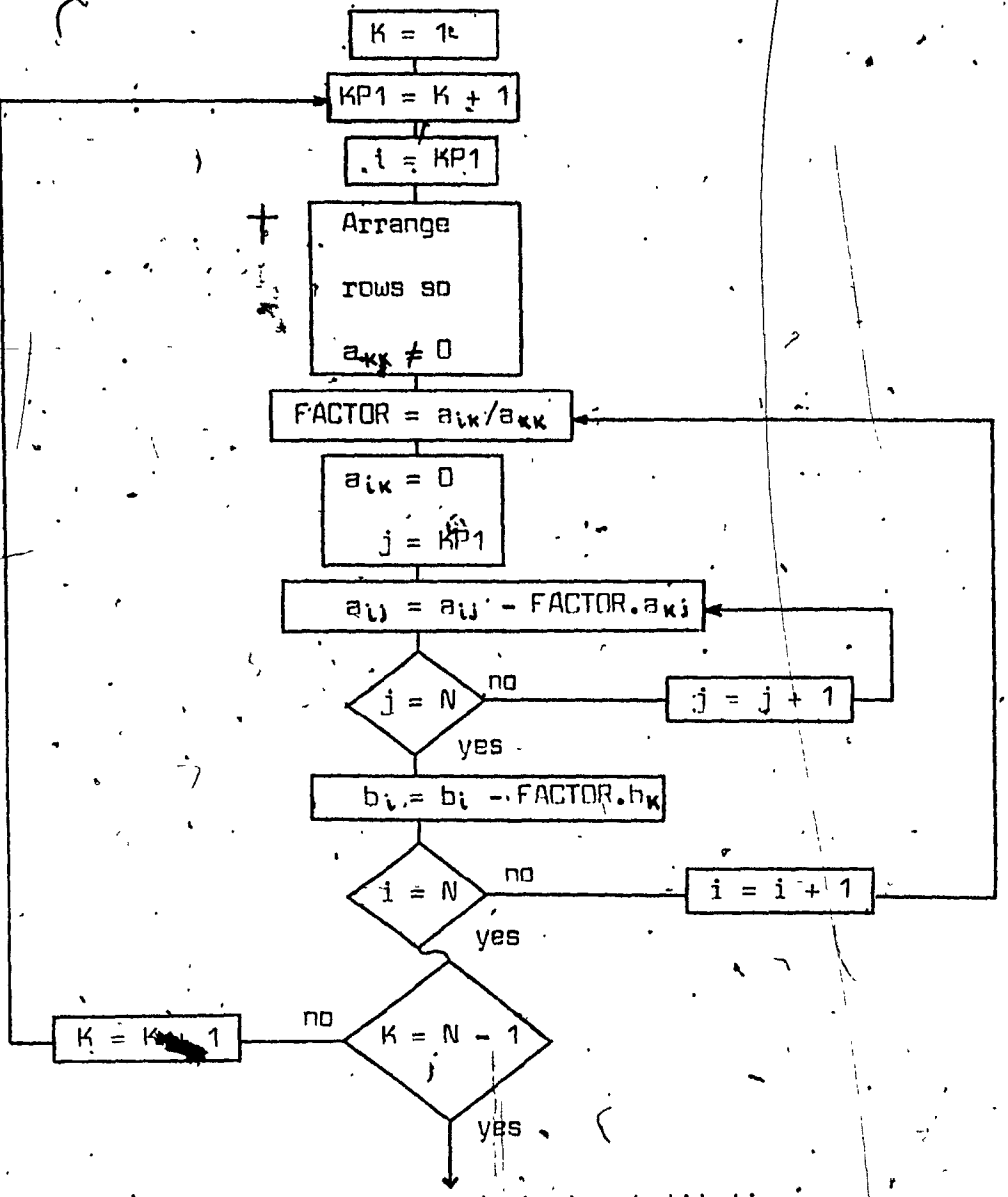

Fig. 6.4

Block diagram of the method Gauss elimination.

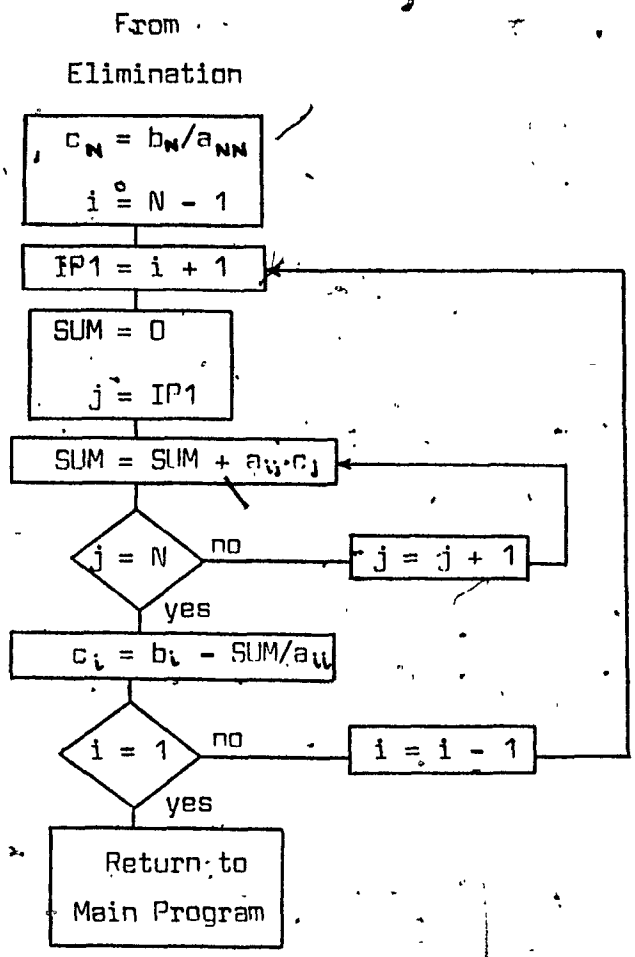

Fig. 6.5

Block diagram of the back substitution in Gauss elimination

largest - in absolute value - of the coefficient in the Kth column is in the Kth row. This is referred to as pivotal condensation.

A block diagram of the testing and if necessary the interchanging is shown in Fig. 6.6 . It should be thought of as replacing the box marked † in Fig. 6.4 . In studying Fig. 6.6 , we recall from Fig. 6.4 that as we enter this phase K has some value and i has just been set to K + 1 . We begin by setting an auxiliary subscript l equal to K. The first comparison is then between a_{lK}, the element just below the diagonal term a_{KK}, and a_{lK}, which is a_{KK}. If a_{lK} is found to be larger in absolute value, we set l = i . The subscript l therefore always represents the row number of the element in the Kth column that is so far the largest one tested. The subscript i runs through all values from K + 1 to N, inclusive. Thus at the end of this loop l identifies the largest element, the one we want for a_{KK} after interchanging if necessary.

Actually, the original a_{KK} could already be the largest. We therefore immediatly test for this possibility and omit the interchanging in that case.

Before returning to the main elimination process, it is necessary to set i back to the value it had before we used it as a subscript in the testing loop. This is easily done : in the main block diagram, Fig. 6.4 , the value of i had just been made K + 1 , which we repeat here.

Interchanging is done on pairs of values, one from row K and one from row l , whatever l may be. The interchange of each pair of values requires a three-step process :

1 we move the first value to a temporary storage location which we call TEMP
2 we move the second value to the location originally occupied by the first
3 we move the first value, which is now in TEMP, to the location originally occupied by the second

This operation must be done on all pairs in the two rows, which is carried out by a loop using j as a subscript. Finally the two constant terms are interchanged and the process is complete.
The listing of GAUSS 2 is in the Appendix.

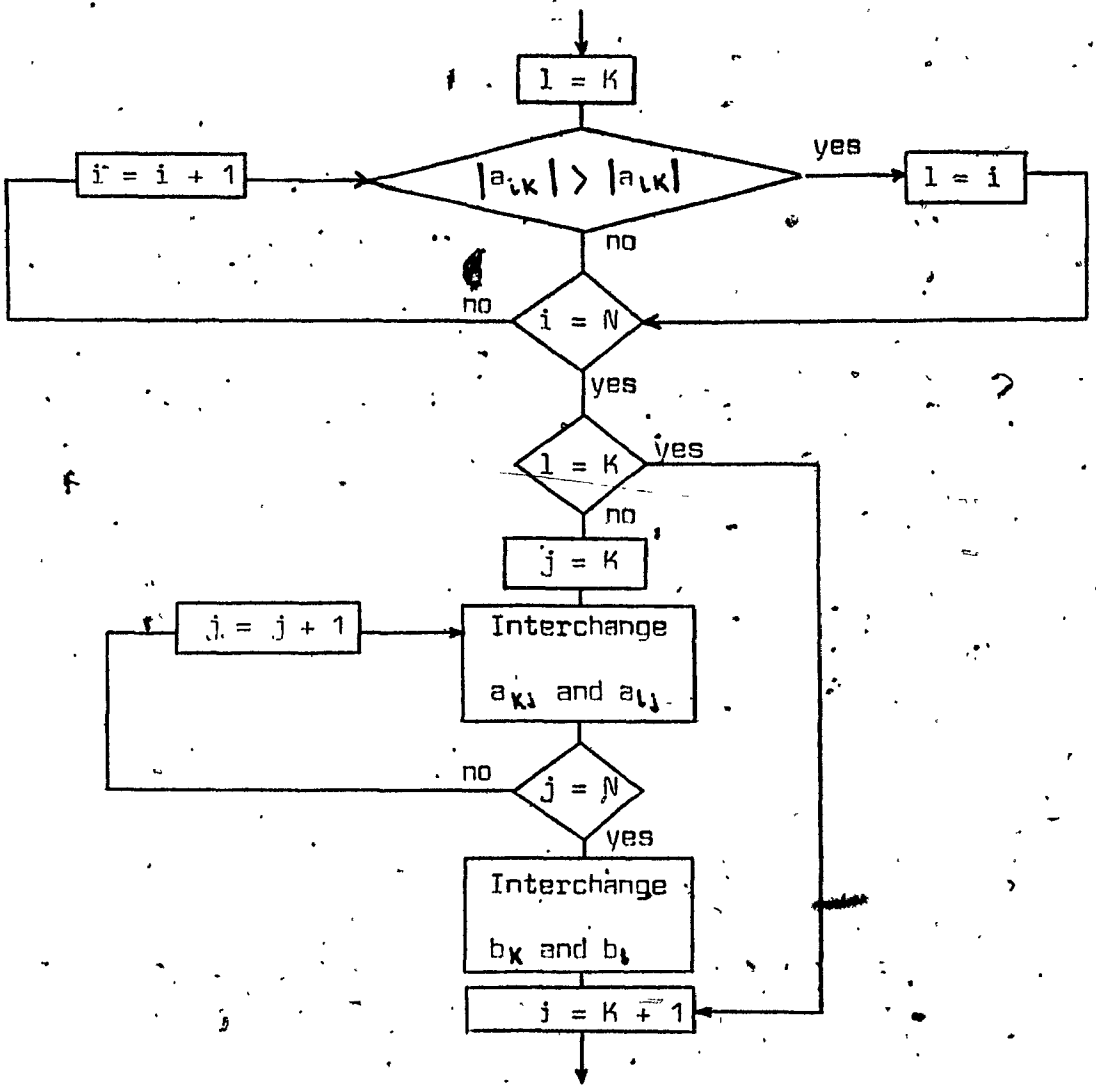

Fig. 6.6

Block diagram of the process of choosing the Kth row and performing a row interchange if necessary.

7. RESULTS

7.1. Energy Calibration

We consider the first five principle gamma-rays from decay of radium and daughters, in Wallace and Conte's table[17]. Comparing these energies with Nuclear Data Tables[18], we observe the same energies except for the first gamma-ray, which is listed 186.0 Kev in Ref.18 instead of 185.7 Kev in Ref.17 . Moreover while other energies are accurately known to five digits, this decay line is only known to four. This prompted our search for an adequate energy calibration method in order to quote the 186 Kev line with a precision of five digits.

There are many methods for obtaining accurate energy calibration.

(1) Using a precision pulser. A pulse generator is calibrated by setting pulse heights to coincide with gamma-ray lines of known energies, whereby in turn the pulser calibrates the spectrum.

(2) A single source which has many transition lines over the region of interest can also be used.

(3) Applying the mixed source method where the transition lines of several sources can be used.

In all cases, as many points as we can obtain are needed for accurate calibration. Now method (1) revealed to us that the ADC was not linear over 95% of scale as specified, and that thermal drift caused energy gain variations affected us. In order to eliminate these energy gain variations the "Analog to Digital Converter" (ADC) was sealed off in a plastic enclosure.

Still, the drift though substantially reduced, was not totally removed. We resolve then to drop the first method and opt mainly for the third one due to lack of sources having the requisite gamma-rays in the 200 Kev region. In the mixed source method we resolved to make short runs for sustained energy accuracy.

The next step is the Gaussian fit of the peaks (hence giving their centroid position) by a program that automatically analyses the entire spectrum, called SPEC . Once this is done, one looks for best fits and enters the centroids and the relative energies into a least squares curve fitting program.

For ^{133}Ba, ^{137}Cs, ^{60}Co and ^{226}Ra, polynomial fits above order three were tried, but little improvement was noted beyond the cubic. The average deviation over a region of 276 to 1332 Kev was .0132 Kev for a cubic fit, .0214 Kev for a quadratic fit and .125 Kev for the linear fit. Repeating the experiment, this time without the ^{226}Ra source we obtained similar results. We decided thus to use a cubic as our energy calibration curve.

For two months this method was to be used extensively in numerous runs. We summarize the effort here and retrace the main features. Shown in Table 7.1 are the energies and relative intensities of the gamma-rays for the sources used (Intensities are peak areas).

Considering runs with only one source, ^{226}Ra, and excluding the 186 Kev peak from the least squares fit, the cubic produced energies that oscillated between 186.18 Kev and 186.14 Kev. In the following mixed sources methods the 186 Kev peak is excluded as before from the least squares fit. For these sources : ^{57}Co, ^{226}Ra, ^{137}Cs, the energy obtained varied between 186.125 and 186.137 Kev. Using ^{182}Ta, ^{226}Ra, ^{137}Cs the energy value was between 186.14 and 186.10 Kev. In runs involving ^{154}Eu, ^{226}Ra, ^{137}Cs values were between 186.16 and 186.14 Kev. Finally in runs with ^{57}Co, ^{133}Ba, ^{226}Ra, ^{137}Cs as sources, and with the ^{133}Ba energy values taken from Aubin and Monaro[19], the energies obtained were 186.12 to 186.16 Kev.

We therefore claim the value of 186.14 ± .04 Kev as being the first principle gamma-ray from radium decay and daughters.

7.2. Relative Detector Efficiency

We intended to use the x-ray in radium decay in order to extend to lower energies the use of ^{226}Ra as an efficiency calibration source. Wallace and Coote claim that because of complex spectral backgrounds, and the rapidly changing efficiency of the detector in this energy region, the x-rays were too remote (from the efficiency corresponding to the 186 Kev gamma-ray) for calibration purposes.

At under .100 Kev, for reliable x-ray or gamma-ray peak area calculations, we have to take into consideration two kinds of attenuations : air absorption and absorption due to the material surrounding the source.

ENERGIES in Kev	RELATIVE INTENSITIES
^{226}Ra[a]	
186.0	7.67
241.92	17.21
295.22	41.86
351.99	81.40
609.4	100
768.4	11.69
934.1	7.21
1120.4	32.56
1238.2	14.88
1377.8	10.70
1385.4	2.40
1729.9	7.44
1764.7	38.60
2118.9	3.02
2204.5	12.56
2448.0	4.12
^{57}Co[a]	
122.07	87
136.43	11
^{133}Ba[a]	
81.0	36
276.3	7.5
302.7	19.6
355.9	62
383.7	9.4

ENERGIES in Kev	RELATIVE INTENSITIES
^{182}Ta[b]	
67.75	119
100.10	40.65
152.43	20.7
222.10	22.8
^{154}Eu[c]	
123.10	111.32
247.92	19.13
591.71	14.63
^{137}Cs[a]	
661.64	100
^{60}Co[a]	
1173.2	99.88
1332.5	100

[a] Ref. 18
[b] Ref. 24
[c] Ref. 19

Table 7.1

Energies and Relative Intensities of gamma-rays for ^{226}Ra, ^{57}Co, ^{133}Ba, ^{182}Ta, ^{154}Eu, ^{137}Cs, ^{60}Co.

We know that interaction of gamma-radiation or x-rays with matter is characterized by the fact that each photon is removed individually from the incident beam in a single event. Thus the number of photons removed ΔB, is proportional to the thickness traversed, Δx, and the number of incident photons, B

$$\Delta B = -\mu B \Delta x \qquad (7.1)$$

where μ the proportionality cst. is called the attenuation coefficient. If the radiation is homogeneous, μ is a constant and the integretion of (7.1) yields

$$B = B_0 \exp(-\mu x) \qquad (7.2)$$

since x is expressed here in cm and since μx must be dimensionless, the attenuation coefficient μ is expressed in cm^{-1}. From a table of gamma-ray attenuation coefficients for dry air[20], μ/ρ, the mass absorption coefficient, (where ρ is the air density) vs photon energy were plotted in order to determine air absorption at the x-ray energies of ^{226}Ra.

Wallace and Coote's estimate of the x-rays, primarily $K\alpha$'s and $K\beta$'s of 76.1 and 87.0 Kev could not be duplicated. A thorough examination of the article entitled ^{226}Ra + (chain of daughters) by Martin and Blichert-Toft in Nuclear Data Tables 1970 shows x-rays from transitions in Bi, Po, Rn. These are shown in table 7.2

	ENERGY IN MEV	INTENSITY
X_K	.07892	22.3
	transition in Bi	
	.08117	1.26
	transition in Rn	
	.09578	0.73
	transition in Rn	

Table 7.2

X_K transitions of radium decay and daughters.

Details on the various $K\alpha$'s (energies and intensities) are obtainable from the Table of Isotopes[21]. They are tabulated in Table 7.3 where energies are in Kev and intensities shown in parentheses.

Z	ELEMENT	K_{α_2}	K_{α_1}	K_{β_2}	K_{β_1}
83	Bi	74.81	77.11	87.2	89.8
		(55)	(100)	(36)	(10)
84	Po	76.86	79.29	89.6	92.4
		(56)	(100)	(36)	(11)
86	Rn	81.07	83.78	94.7	97.6
		(56)	(100)	(37)	(11)

Table 7.3

. K transitions for Bi, Po, Rn .

The x-ray peaks are complex and separated in two; K_α's for the lower energies, K_β's for the higher. Some K_α values are now calculated from weighted averages. Taking into account transitions in Bi only, the average K_α energy is 76.29 Kev. Taking into account transitions in both Bi and Po yields an energy of 76.41 Kev , while including transitions in Bi, Po and Rn, the average energy is 76.60 Kev.

When using the energy calibration method described in 7.1. we obtain 76.52 Kev for the experimental K_α value. A 0.08 Kev discrepancy (or twice the error for the 186 Kev line) may be due mainly to : errors in intensities as quoted by Martin and Blichert-Toft; also x-ray intensities being weaker than the gamma-rays' they necessitate longer runs (hence increased thermal drift). The respective mass absorption coefficients μ/ρ for the average x-ray energies are : .167 cm^2/g for the 76.60 Kev region and .158 cm^2/g for the 88.12 Kev region.

We can rewrite (7.2) as :

$$B = B_0 \exp(-\mu/\rho \cdot \rho \cdot x) \qquad (7.3)$$

where ρ the density of air will depend on the conditions of each run. The mass of dry air is given by

$$m = V.a. \frac{H}{76} \cdot \frac{273.15}{T} \qquad (7.4)$$

where V = volume expressed in cm^3

a = 1.293 g/cm^3 , the density at standard conditions (°C, 76 cm)

H = pressure in cm of Hg

T = absolute temperature in °K

From (7.4), the density for air for individual runs is :

$$\frac{m}{V} = \rho = a \cdot \frac{H}{76} \cdot \frac{273.15}{T} \qquad (7.5)$$

Some sources are encapsulated in plastic, so that scattering in the material surrounding them has to be considered. For the ^{226}Ra x-rays, three runs were performed and the fitted areas for the K_α peak averaged. Taking the same source, we now add an extra layer of material of same thickness in front of the source and average again the K_α area over three runs.

With only one thickness the number of recorded photons is

$$B_1 = B_0 \exp(-\mu x)$$

with twice the thickness this number becomes

$$B_2 = B_0 \exp(-2\mu x)$$

we evaluate the ratio

$$B_1/B_2 = \exp(\mu x) \qquad (7.6)$$

the term on the right could be called an "attenuation factor". This factor yielded a value of 1.0062 . Now rewriting (7.2) as

$$B_0 = B \exp(\mu x)$$

the incoming number of photons B_0 , can easily be obtained from the attenuated number B times the empirically found "attenuation factor", $\exp(\mu x)$.

In many gamma decay transitions electrons are emitted along with gamma-rays. The electron is ejected through the process of internal conversion, by the direct transfer of energy from the nucleus to the electron through the Coulomb interaction between the two. The ratio of the probability for emitting an electron from a given shell to the probability for emitting a gamma-ray is called the internal conversion coefficient α. Furthermore α_K is the value of α for the emission of a K shell electron. Also, the fluorescence yield for the K atomic shell ω_K, is defined as the probability that a vacancy in that shell will result in the emission of an x-ray.

The method used in the calibration of the relative detection efficiency for the Ge(Li) detector is the pair point method. This method relies on the values of relative gamma ray emission rates T_{γ_i}

and T_{γ_2} for pairs of gamma rays ; from a comparison of the full energy peak areas $A(E_1)$ and $A(E_2)$, and using the known emission rates, the relative detection efficiency $RDE(E_1,E_2)$ can be determined

$$T_{\gamma_1} . RDE(E_1) = A(E_1)$$

$$T_{\gamma_2} . RDE(E_2) = A(E_2)$$

hence $$RDE(E_1,E_2) = \frac{A(E_1)}{A(E_2)} \cdot \frac{T_{\gamma_2}}{T_{\gamma_1}} \qquad (7.7)$$

The probability for K x-ray emission following an internal conversion T_{KX} (IC) is related to the probability for gamma T_γ by

$$T_{KX}(IC)/T_\gamma = \alpha_K \omega_K$$

where α_K is the internal conversion coefficient and ω_K is the K fluorescence yield. Now the peak areas of the K x-rays and gamma-rays are related to the relative detection efficiencies in this manner

$$T_{KX}(IC) . RDE(X) = A_X$$

$$T_\gamma . RDE(\gamma) = A_\gamma$$

where A_X is the area of the K_α + the area of the K_β peak. We relate now the relative detection efficiency of the x-ray to the RDE of the gamma-rays by :

$$RDE(X) = RDE(\gamma) . (A_X/A_\gamma) . T_\gamma/T_{KX}(IC) \qquad (7.8)$$

In this modified pair point technique we try two sources which involve de-excitation from only one level in the daughter nucleus ^{203}Hg and ^{137}Cs. The daughter nuclei are ^{203}Tl and ^{137}Ba.

Energies in KeV and relative intensities of the K_α x-rays taken from Ref. 21 are shown in Table 7.4 below

Z	ELEMENT	$K_{\alpha 2}$	$K_{\alpha 1}$	$K_{\beta 1}$	$K_{\beta 2}$	ω_K
81	Tl	70.83	72.87	82.5	84.9	.95
		(55)	(100)	(35)	(10)	
56	Ba	31.82	32.19	36.4	37.3	.88
		(52)	(100)	(20)	(6)	

Table 7.4

The respective K_α spectra of ^{203}Tl and ^{137}Ba are shown in Fig. 7.1,7.2. While ^{203}Tl x-rays were fitted the more compressed ^{137}Ba x-rays proved to be a problem. This is mainly due to the existence of backscatter peaks in the background. Using (4.7) the $K_{\beta 1}$ and $K_{\alpha 1}$ contribute respectively to backscatter peaks of 31.81 and 28.59 Kev. The proximity of these energies with those of the K_α's, made accurate background subtraction impossible, and ^{137}Cs could not be used as a reliable source.

One of our goals is to extend to lower energies the use of ^{226}Ra as a calibration source. The graph in Fig. 7.3 shows in detail the RDE for energies below 609 Kev.†

We start to plot the graph using ^{226}Ra runs and applying the pair point method. The 609 Kev peak is assigned a RDE of 1 and is the peak to which all others are compared. The RDE curve also depends on whose relative peak intensities are used. A comparaison of RDE values according to several authors is shown in Table 7.5 below.

ENERGY in Kev	RDE WALLACE-COOTE[17]	RDE N.DATA[18]	RDE GROMOW[22]	RDE MOWAT[23]
186.14	4.268	5.515	4.449	5.159
241.92	3.140	3.527	3.747	3.770
295.22	2.350	2.685	2.799	2.712
351.99	1.966	2.106	2.180	2.151
609.4	1	1	1	1

Table 7.5

At this point two possibilities occur : either the curve goes through Ref. 17 values which appear to be on their own, or through the three other Refs. values which group at systematically higher values. In Ref. 17 relative intensities were obtained from an average of the results of four detectors, giving credence to the results.

† From here on, whenever quoting runs for each source, three runs are performed each time and the tabulated RDE stands for the average value.

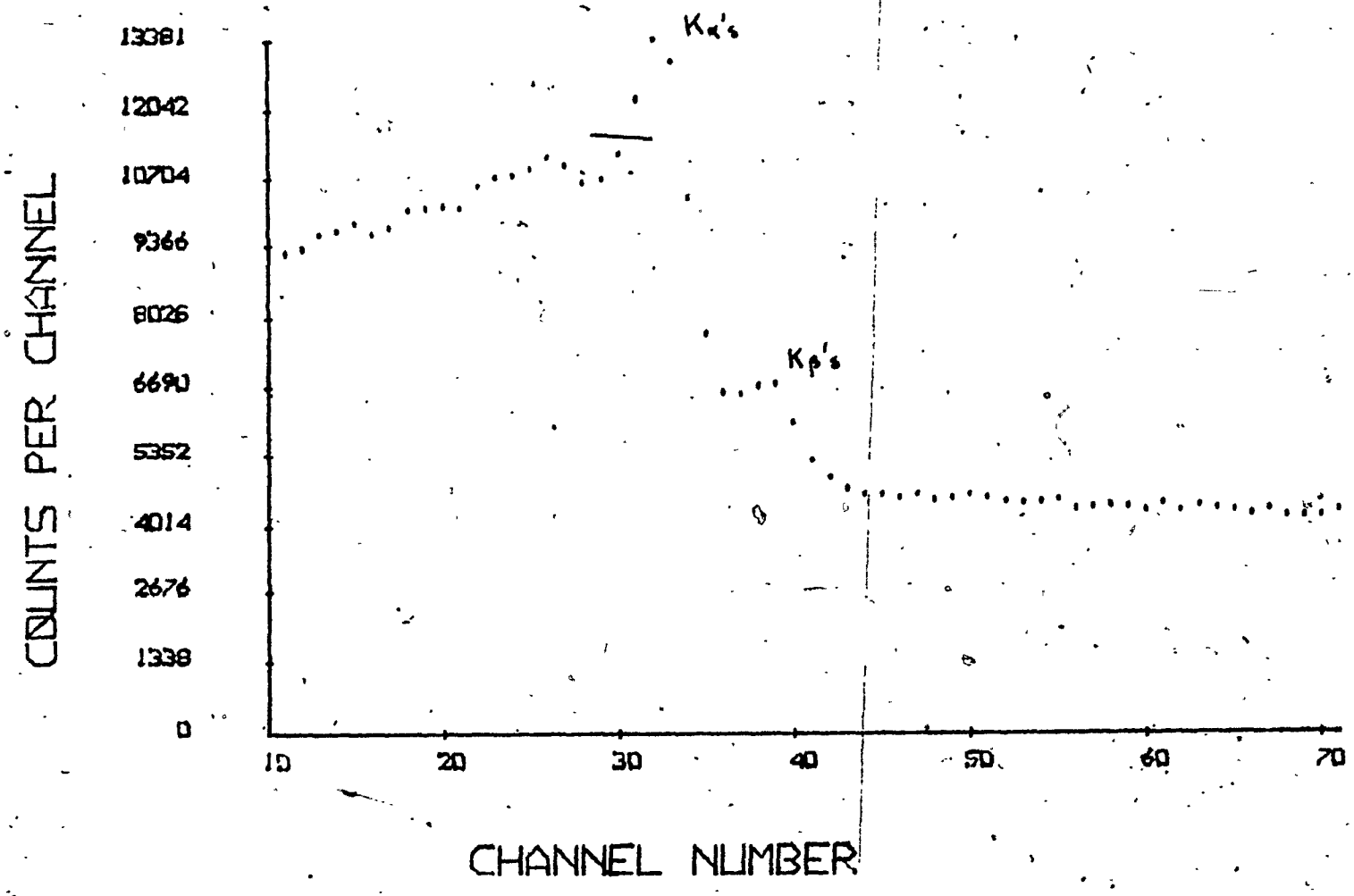

Fig. 7.1

X-rays of ^{137}Ba

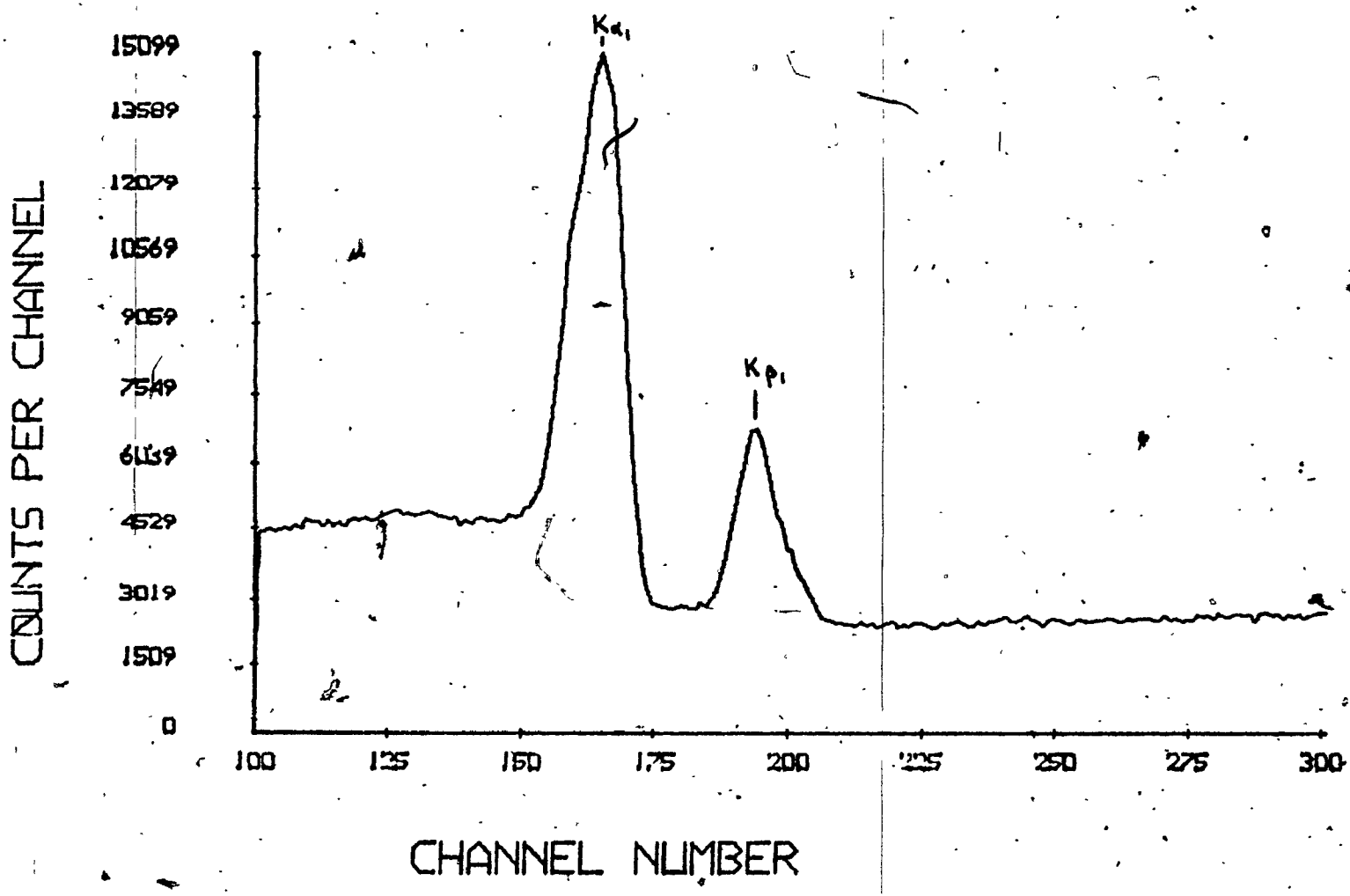

Fig. 7.2
X-rays of ^{203}Tl

Fig. 7.3

Relative Detector Efficiency (RDE) vs Energy in Kev

^{226}Ra { × Wallace and Coote; □ Nuclear Data 1970; ○ Gromow; △ Mowatt

^{154}Eu ⊙

^{182}Ta +

^{133}Ba •

^{203}Hg ■

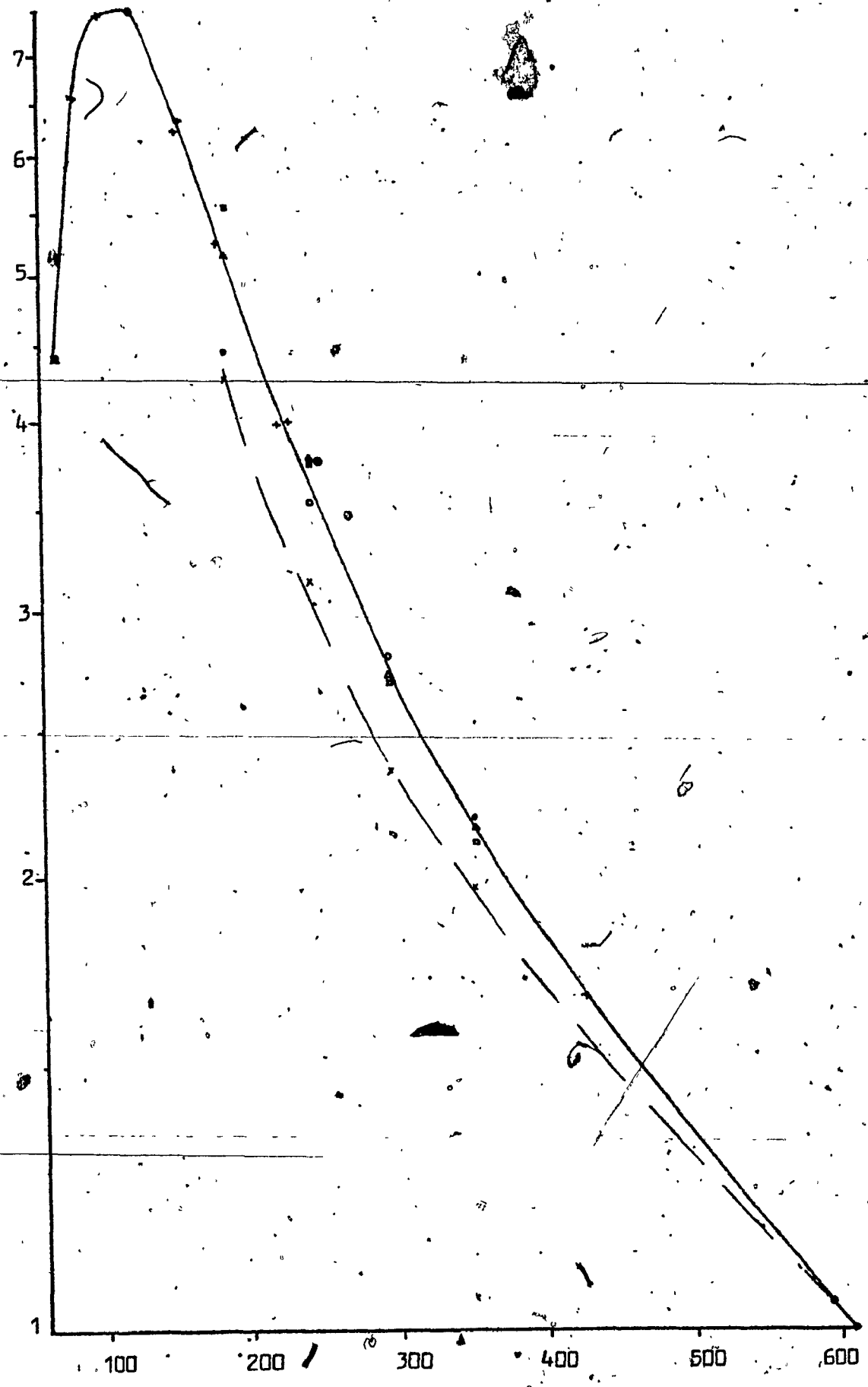
7
6
5
4
3
2
1
100
200
300
400
500
600

If we do not adopt Wallace and Coote's data, some justification will be required. To do so on a solid basis, we perform ^{154}Eu runs and use the relative intensities as given by Auhin and Monaro[19]. Again we apply the pair point method basing ourselves on the 592 Kev transition. Since the RDE of 1 is already assigned to the 609 Kev line, the 592 Kev (for either RDE curve) has a RDE value of 1.04 . The other energies are plotted with respect to this value according to Table 7.6

ENERGY in Kev	RDE FOR $^{154}Eu^{19}$	RDE ASSIGNED ON GRAPH
123.10	7.193	7.481
247.92	3.648	3.763
591.71	1	1.04
602.42	.818	.851

Table 7.6

The last transition's RDE is plotted on the 0-2.5 Mev energy range graph of ^{226}Ra shown in Fig. 7.4 . The crucial 247.92 Kev transition causes us to use the upper curve drawn through Mowatt's values. In order to draw a smooth curve in the region where the RDE curve turns over, more points are needed on the graph of Fig. 7.3 . We note that ^{182}Ta has many useful transitions in the 84 to 264 Kev range. Some of these appear as complex peaks but can be dealt with by our double peak fitting program GAUSS 2 . Using Whites' average relative intensities[24], and basing ourselves on the 264 Kev transition, the RDE values are obtained in Table 7.7 .

The intense 87 Kev transition of ^{154}Eu could not be fitted accurately since its energy coincides with the K_{β_1} x-ray of ^{182}W . Nevertheless we do have a point as low as 84.7 Kev . As an extra check, since the source is readily available, we performed several runs of ^{133}Ba . The average 80.89 Kev peak is compared to the 355.9 Kev transition. From tables of Ref. 25 we obtain Table 7.8 .

Fig. 7.4

Relative Detector Efficiency, 0-2.5 Mev Energy Range

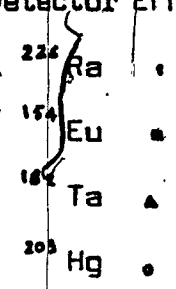

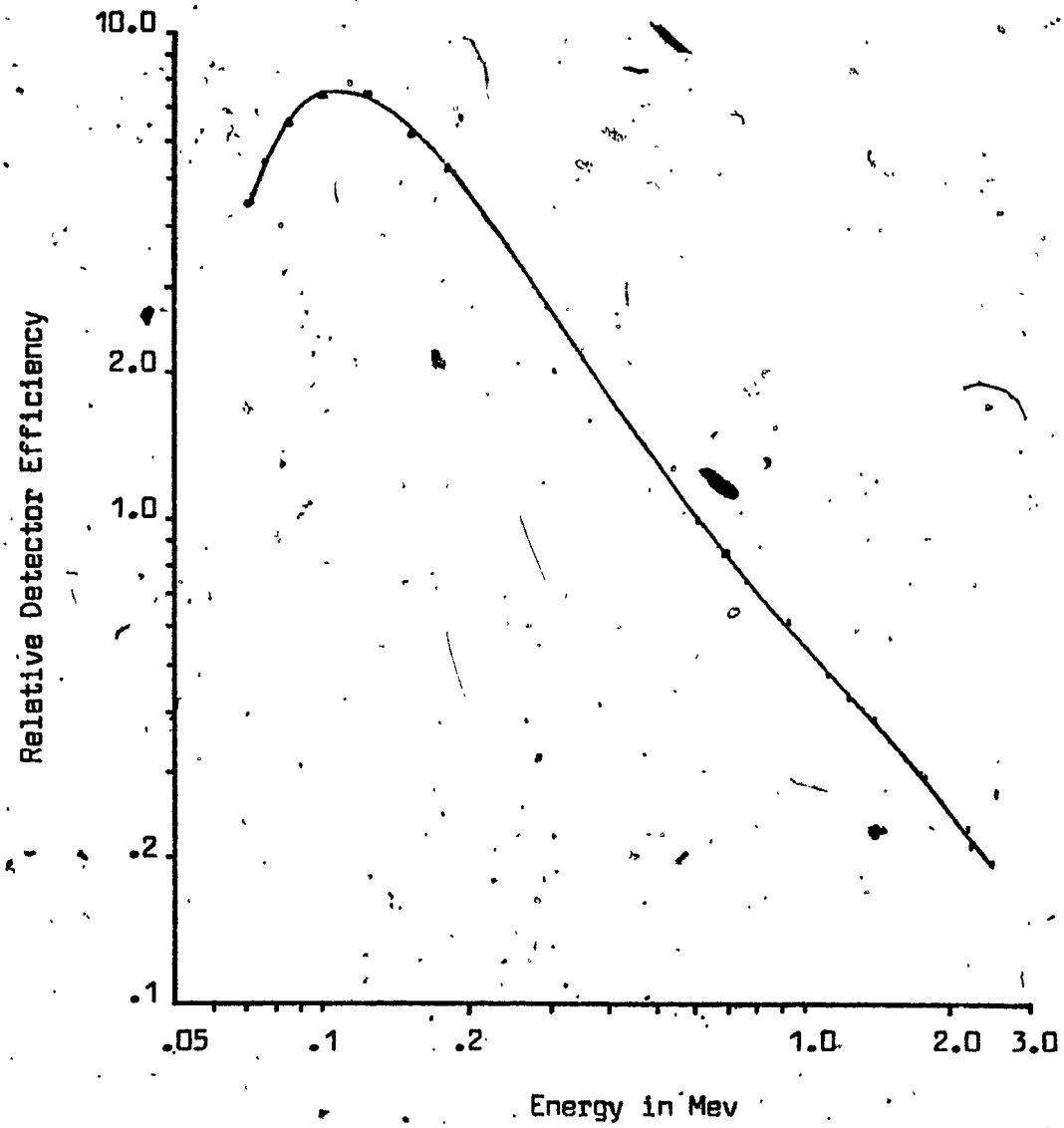
10.0
2.0
1.0
.2
.1
Relative Detector Efficiency
.05
.1
.2
1.0
2.0
3.0
Energy in Mev

ENERGY in Kev	RDE FOR $^{182}Ta^{24}$	RDE ASSIGNED ON GRAPH
84.678	2.035	6.56
100.101	2.302	7.425
† 152.429	1.926	6.21
† 156.389	1.961	6.326
179.392	1.628	5.249
† 222.104	1.228	3.96
† 229.317	1.245	4.016
264.068	1	3.225

† Complex Peak

Table 7.7

ENERGY in Kev	RELATIVE INTENSITIES	RDE FOR $^{133}Ba^{25}$	RDE ASSIGNED ON GRAPH
79.6	4.54		
80.89		3.106	6.59
81.0	53.73		
355.9	100	1	2.12

Table 7.8

Finally applying the modified pair point method to the ^{203}Hg runs we obtain Table 7.9

ENERGY in Kev	RDE FOR $^{203}Hg^{21}$	RDE ASSIGNED ON GRAPH
70.83	1.487	4.42
279.2	1	2.97

Table 7.9

We restrict ourselves to the K_α peak since it showed less variation from its average RDE value. Now from the RDE curve obtained in this

way we can determine "the relative emission rate" or relative intensity of the Kα's of ^{226}Ra decay. For a Kα energy of 76.60 Kev a RDE of 5.4 is obtained from the graph. Whatever the reference the 609 Kev transition in ^{226}Ra is the main one, and has a relative intensity of 100 . Hence replacing in (7.8) the RDE of the Kα's, RDE(X) by 5.4 yields an average value for relative intensity of 44.03.

During the course of this work an updated Nuclear Data Tables[25] became available. At this time Mowatt was believed to have the most precise data on ^{226}Ra relative intensities available. It is noteworthy that he was cited as a reference in Ref. 25 . However Ref. 25 is an average of many works (one privately communicated, another concerning Rn decay without error evaluation for intensities) it is felt that Mowatt's values remain the best for the 186-609 Kev region.

Above 609 Kev, however, Mowatt contributes only one point and so Ref. 25 can be considered as data independent from Mowatt's.

We now consider the choices available for the higher energy region. The references left are Wallace and Coote[17] and the thorough table of Gromow[22] . What we have witnessed for under 609 Kev makes us cautious about Ref. 17 . In this lower energy region Ref. 22 agreed well with Mowatt except for the 186 Kev transition. In Table 7.10 , we quote energies from Ref. 25 . The relative intensities and RDE values of Ref. 22 and Ref. 25 are shown, for energies of 609 Kev and over.

As observed, the RDE values of Gromow and Ref. 25 are quite close except for over 2 Mev where Gromow's values tend to curve down. For this energy region we check with Dzhelepov, a reference of Gromow. The latter's relative intensities are closer to those of Nuclear Data and this caused us to choose Ref. 25 RDE values for the .609-2.448 Mev region.

In Fig. 7.5 the cubic background of x-rays for radium decay is shown, while Fig. 7.6 shows the complete spectrum of ^{226}Ra .

Fig. 7.5

Shown are the complex K_α's and K_β's x-ray peaks of radium decay, with a cubic background fitted.

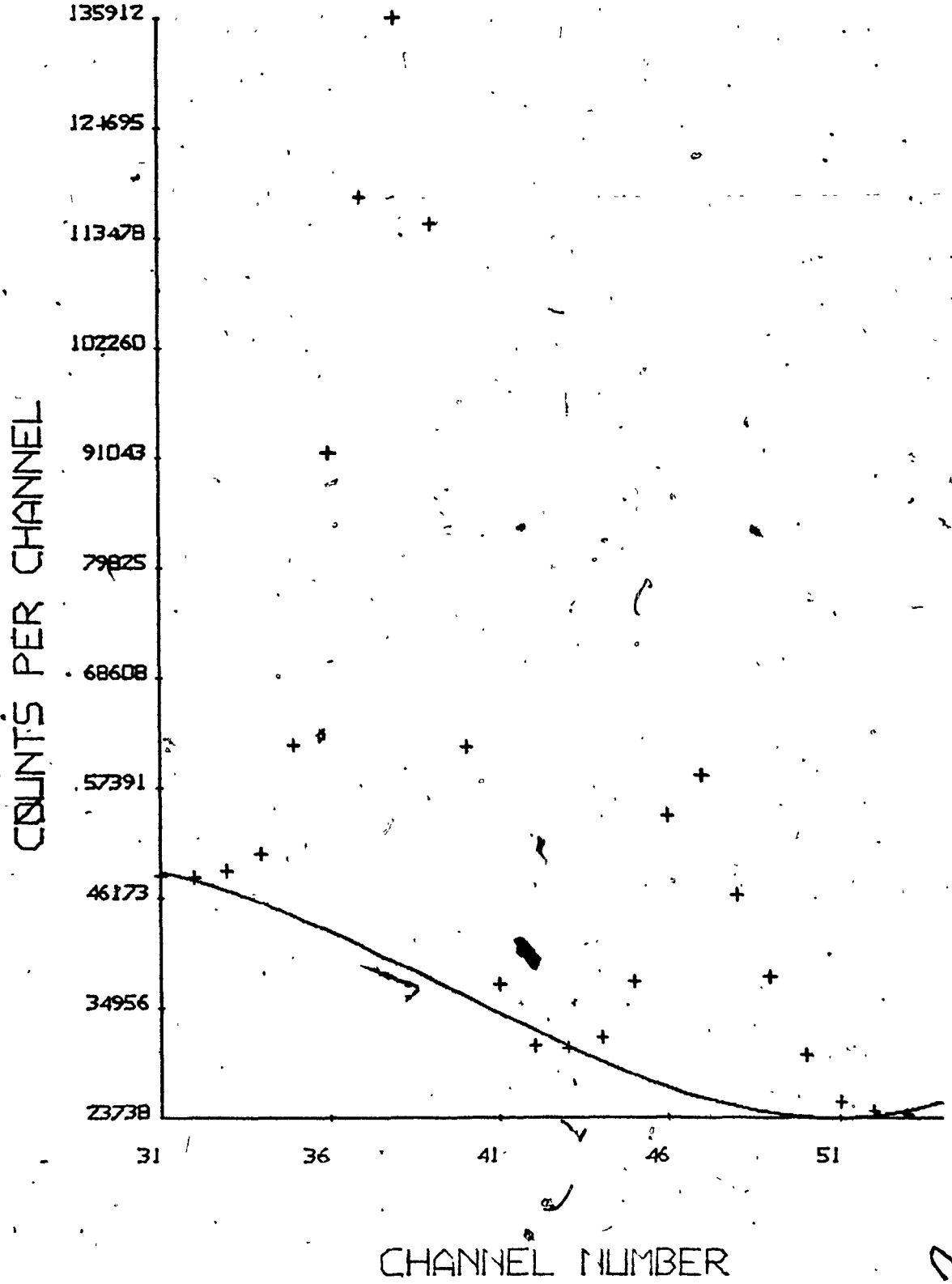
135912
124695
113478
102260
91043
79825
68608
57391
46173
34956
23738
COUNTS PER CHANNEL
31
36
41
46
51
CHANNEL NUMBER

Fig. 7.6

Complete ^{226}Ra spectrum, note the 13.4 expansion factor at channel 480

ENERGIES	NUCLEAR DATA[25]		K.GROMOW[22]	
in Mev	RELATIVE INTENSITIES	RDE	RELATIVE INTENSITIES	RDE
.6092	100	1	100	.1
.7684	10.99	.748	10.60	.775
.9341	6.90	.620	6.99	.612
1.1203	30.06	.477	29.41	.536
1.2381	12.81	.433	12.75	.435
1.3776	8.64 } 10.42	.393	9.04 } 10.70	.383
1.3853	1.78 }		1.66 }	
1.7296	6.34	.298	6.58	.287
1.7645	34.30	.284	34.36	.284
2.1184	2.54	.231	2.61	.225
2.2041	10.95	.211	11.38	.203
2.4476	3.41	.196	3.79	.176

Table 7.10

Comparing two references' relative intensities and RDE for ^{226}Ra

Upon examination of Fig. 7.4 , three sources are needed for the .0766 - 2.4476 Mev energy calibration range ; ^{226}Ra useful down to the .0766 Mev energy of the K_{α} peak, ^{182}Ta for the important region where the RDE turns over, from .0847 to .1794 Mev, and finally ^{154}Eu in order to obtain the .1231 Mev point, eliminating a gap left by the ^{182}Ta . Another very convenient source for use, if one is to use a fourth source, is ^{125}Sb. This source has a long half-life (2.7 years) and several major transitions from .176 to .671 Mev. This source will yield four extra points on the graph in the .380 - .600 Mev region where ^{226}Ra left a void. However, since the RDE curve is slowly varying over the void, it was felt unnecessary to use a fourth source in this work. We list in Table 7.11 energies, relative intensities and their errors, for the pair point method.

	ENERGIES in Kev	RELATIVE INTENSITIES	RELATIVE ERRORS
^{226}Ra(a)	186.18	8.20 ± .12	1.46%
	242.	16.1 ± .21	1.30%
	295.2	41.45 ± .56	1.35%
	351.96	79.7 ± 1.1	1.38%
	609.19	100.	—
^{154}Eu(b)	123.10	123.32 ± 3.31	2.97%
	591.71	14.63 ± .33	2.26%
^{182}Ta(c)	84.678	7.64 ± .37	4.84%
	264.068	10.7 ± .4	3.74%

No errors available for ^{133}Ba relative intensities.

(a) Ref. 23

(b) Ref. 19

(c) Ref. 24

Table 7.11

Let us consider the general problem of propagation of errors. If G is to be calculated from measurements designated $M_1, M_2, \ldots M_n$, we can write it as $f(M_1, M_2, \ldots M_n)$ and we mean by $\partial f/\partial M_i$ the partial derivative with respect to the variable M_i. Pugh and Winslow[26] prove the following relation where the values of σ (standard deviation) are for the averaged $G, M_1, M_2, \ldots M_n$

$$\sigma_G^2 = \left(\frac{\partial f}{\partial M_1}\sigma_1\right) + \left(\frac{\partial f}{\partial M_2}\sigma_2\right) + \ldots + \left(\frac{\partial f}{\partial M_n}\sigma_n\right) \quad (7.9)$$

for the special case in which

$$G = M_1^a M_2^b M_3^c \ldots \quad (7.10)$$

if one applies (7.9) to the case of three variable factors, we obtain

$$\sigma_G^2 = \left(a M_1^{a-1} M_2^b M_3^c \sigma_1\right)^2 + \left(b M_1^a M_2^{b-1} M_3^c \sigma_2\right)^2 + \left(c M_1^a M_2^b M_3^{c-1} \sigma_3\right)^2$$

Dividing the left-hand side of this relation by the square of the left-hand side of (7.10) and the right-hand side by the square of the right-hand side of (7.10), the result is

$$\left(\sigma_G/G\right)^2 = \left(a\,\sigma_1/M_1\right)^2 + \left(b\,\sigma_2/M_2\right)^2 + \left(c\,\sigma_3/M_3\right)^2 \quad (7.11)$$

where the σ_G/G, σ_1/M_1, etc., are the relative or fraction errors.

We now evaluate possible errors affecting the efficiency curve in Fig. 7.3

For ^{154}Eu 123 Kev peak, its RDE(E_1) is related to the RDE(E_2) at 597 Kev. We rewrite (7.7) as

$$RDE(E_1) = RDE(E_2) \cdot \frac{A(E_1)}{A(E_2)} \cdot \frac{T(E_2)}{T(E_1)} \qquad (7.12)$$

There are three factors or terms on the right-hand side of (7.12). Once the error for each factor is determined, we utilize (7.11) to obtain the relative detector efficiency of RDE(E_1).

(1) The uncertainty in the first term of (7.12) is Mowatt's average error of 1.37% for the 609 to 186 Kev region.

(2) The uncertainty in the second term stems from the statistical fluctuations of the area ratios. Applying (3.10) the relative errors amounted to 1.05% .

(3) The third term has uncertainties on the two transmission probabilities (or relative intensities) ; for the 121.10 and 591.71 Kev lines they are respectively 2.97 and 2.26% . From (7.11), $T(E_2)/T(E_1)$ has then an estimated relative error contribution of :

$$((2.97)^2 + (2.26)^2)^{1/2} = 3.73\%$$

We use now (7.11) and insert the errors of each term to obtain the estimated relative error of the RDE for the 123.10 Kev line. This is

$$((1.37)^2 + (1.05)^2 + (3.73)^2)^{1/2} = 4.11\%$$

Considering ^{182}Ta 84.68 Kev transition, the RDE is calculated in the same manner and yields an estimated relative error of 6.61% .

For the $K\alpha_1$ transition of ^{203}Hg decay, the RDE(X) is obtained using (7.8), this yields an estimated relative error in RDE(X) of 2.37% .

Since the 76.60 Kev energy of ^{226}Ra decay is between the 84.68 Kev transition in ^{182}Ta and the 70.83 Kev $K\alpha_1$ energy of ^{203}Hg decay, the RDE for this region will be known to an average uncertainty of 4.49% . In Fig. 7.3 , the RDE value for $K\alpha$'s is graphically determined as 5.4 . Now using (7.7) we obtain

$$RDE(E_X, E_\gamma) = 5.4 = \frac{A_X}{A_\gamma} \cdot \frac{T_\gamma}{T_X} \qquad (7.13)$$

As before, to evaluate errors for the area ratio, we apply (3.10) and a relative error of 1.75% is obtained. However, we rewrite (7.13) as

$$\frac{T_\gamma}{T_x} = RDE(E_x, E_\gamma) \cdot \frac{A_\gamma}{A_x} \qquad (7.14)$$

Using (7.11), the relative uncertainty of T_γ/T_x squared is equal to the sum of the squares of the relative errors of each factor in the right-hand side of (7.14). Thus for the relative transition rate, the estimated relative error is :

$$\left((4.49)^2 + (1.75)^2 \right)^{1/2} = 4.82\%$$

And the K_α's relative emission rate becomes : 44.03 ± 2.12

Some authors determine the shape of the efficiency curve by developing a formula for it. Both Harvey[27] and Freeman[28] advocate semiempirical formulae for their relative efficiency curve. Unfortunately when considered by Seyfarth[29], these formulae yield efficiency curves that are either too low or not in agreement with the experimental curve. Furthermore they are restricted to a 500 to 1500 Kev energy range. A functional dependence of our curve would be quite complex, and it was not attempted, although a quadratic in log E vs log RDE would suffice above 200 Kev.

7.3. Conclusion

To summarize, the double Gaussian fitting routines performed well whatever the situation. Furthermore, whether the unresolved peaks rested on a straight or complex background, peak areas proved to be very consistent for the several runs and compared quite favorably with the theoretical relative intensities. Another use of routines can be found in energy calibration where exact centroid position of peaks is important. Our $186.14 \pm .04$ Kev energy is being given credibility by the recently published 186.1 Kev energy of Ref. 25 over the previously quoted energy of 186.0 Kev . Finally due to our reliance on other authors relative intensity values, our worst error of 6.61% in relative efficiency is still well ahead of 15% errors as quoted by Donnelly[12] .

APPENDIX

Computer listing of program GAUSS 2

```
      PROGRAM GAUSS2(TAPE1,TAPE2,OUTPUT)
      DIMENSION X(2048),Y(2048),YC(100),PX(100),B(6),C(6),D(6,6),
     +PU(100),DPU(100)
      COMMON/1/X,Y,M,NUMBER,NL1,NL2,NR1,NR2,B,C,D
  100 FORMAT(/6X,F4.1,I5)
  150 FORMAT(10F7.)
  151 FORMAT(6XF2.,F6.)
  575 FORMAT(9(/6XI4))
  576 FORMAT(4(6XE13.7/))
      READ(1,100)SIGMAO,N
      SIGI=SIGMAO
*
      READ(1,575)NL1,NL2,NPL,NP1,NP2,NPR,NR1,NR2,NXX
      READ(2,150)(Y(I),I=1,N)
      DO 10 I=1,N
      X(I)=I
   10 CONTINUE
      NUMBER=NL2-NL1+NR2-NR1+2
      IF(NXX)366,365,366
  366 READ(1,576)(C(I),I=1,4)
      GO TO 266
  365 M=3
*
      CALL GSS
  266 DO 48 I=NL1,NR2
      XI=X(I)
      YI=Y(I)
      YC(I)=YI-C(1)-C(2)*XI-C(3)*XI**2-C(4)*XI**3
   48 CONTINUE
      CO=YC(NP1)
      DO=YC(NP2)
      XMU1=X(NP1)
      XMU2=X(NP2)
      SIGMAO=SIGI
      JX=1
      M=5
*
   15 DO 20 I=1,M
      B(I)=0.0
      C(I)=0.0
      DO 20 J=1,M
   20 D(I,J)=0.0
*
      DO 30 I=NPL,NPR
      XI=X(I)
      YCI=YC(I)
      ARG1=(XI-XMU1)**2/(2.0*SIGMAO**2)
      ARG2=(XI-XMU2)**2/(2.0*SIGMAO**2)
      DPDC=EXP(-ARG1)
      DPDD=EXP(-ARG2)
      A1=CO*(XI-XMU1)/SIGMAO**2
      A2=DO*(XI-XMU2)/SIGMAO**2
      DPDMU1=A1*EXP(-ARG1)
```

```
      DPDMU2=A2*EXP(-ARG2)
      B1=C0*(XI-XMU1)**2/SIGMA0**3
      B2=D0*(XI-XMU2)**2/SIGMA0**3
      DPDSIG=B1*EXP(-ARG1)+B2*EXP(-ARG2)
      PXI=C0*EXP(-ARG1)+D0*EXP(-ARG2)
      RI=PXI-YCI
*
      B(1)=B(1)-RI*DPDC
      B(2)=B(2)-RI*DPDSIG
      B(3)=B(3)-RI*DPDMU1
      B(4)=B(4)-RI*DPDD
      B(5)=B(5)-RI*DPDMU2
*
      D(1,1)=D(1,1)+DPDC**2
      D(1,2)=D(1,2)+DPDSIG*DPDC
      D(1,3)=D(1,3)+DPDMU1*DPDC
      D(1,4)=D(1,4)+DPDD*DPDC
      D(1,5)=D(1,5)+DPDMU2*DPDC
*
      D(2,2)=D(2,2)+DPDSIG**2
      D(2,3)=D(2,3)+DPDMU1*DPDSIG
      D(2,4)=D(2,4)+DPDD*DPDSIG
      D(2,5)=D(2,5)+DPDMU2*DPDSIG
*
      D(3,3)=D(3,3)+DPDMU1**2
      D(3,4)=D(3,4)+DPDD*DPDMU1
      D(3,5)=D(3,5)+DPDMU2*DPDMU1
*
      D(4,4)=D(4,4)+DPDD**2
      D(4,5)=D(4,5)+DPDMU2*DPDD
*
   30 D(5,5)=D(5,5)+DPDMU2**2
*
      DO 40 I=1,M
      DO 40 J=1,M
   40 D(J,I)=D(I,J)
*
      CALL GSS
      DELC=C(1)
      DELSIG=C(2)
      DELMU1=C(3)
      DELD=C(4)
      DELMU2=C(5)
      PRINT 741,JX
  741 FORMAT(//*DELC/DELSIG/DELMU1/DELD/DELMU2*10X*ITERATION
     +*I2)
      PRINT 742,DELC,DELSIG,DELMU1,DELD,DELMU2
  742 FORMAT(5(E11.3))
*
      TEST=0.00001
      AXE=50.0
      IF(DELSIG)1,1,2
    1 DELTS=-DELSIG
```

```
      GO TO 3
    2 DELTS=DELSIG
    3 IF(DELTS-AXE)31,86,86
   31 IF(DELTS-TEST)4,4,11
*
    4 IF(DELMU1)6,6,7
    6 DELTM1=-DELMU1
      GO TO 8
    7 DELTM1=DELMU1
    8 IF(DELTM1-TEST)9,9,11
*
    9 IF(DELMU2)110,110,112
  110 DELTM2=-DELMU2
      GO TO 113
  112 DELTM2=DELMU2
  113 IF(DELTM2-TEST)120,120,11
*
  120 IF(DELC)122,122,123
  122 DELTC=-DELC
      GO TO 124
  123 DELTC=DELC
  124 IF(DELTC-TEST)130,130,11
*
  130 IF(DELD)131,131,132
  131 DELTD=-DELD
      GO TO 133
  132 DELTD=DELD
  133 IF(DELTD.GT.1000.)GO TO 5
      IF(DELTD-TEST)5,5,11
*
   11 SIGMAO=SIGMAO+DELSIG
      SIGTEST=ABS(SIGMAO)
      IF(SIGTEST-0.2)5,5,17
   17 XMU1=XMU1+DELMU1
      XMU2=XMU2+DELMU2
      CO=CO+DELC
      DO=DO+DELD
      IF(JX-39)16,16,5
   16 JX=JX+1
      GO TO 15
    5 XYZ=2.0*ALOG(2.0)
      FWHM=ABS(2.0*SIGMAO*SQRT(XYZ))
      IF(FWHM.GT.50.0.OR.FWHM.LT.0.5)GO TO 86
*
      COUNTS=AREA=0.0
      DO 232 I=NL1,NR2
      XI=X(I)
      YI=Y(I)
      ARG1=(XI-XMU1)**2/(2.0*SIGMAO**2)
      ARG2=(XI-XMU2)**2/(2.0*SIGMAO**2)
      PXI=CO*EXP(-ARG1)+DO*EXP(-ARG2)
      PX(I)=PXI
      PU(I)=PXI+Y(I)-YC(I)
```

```
S:53 L:53
      DPU(I)=Y(I)-PU(I)
      IF(I.LT.NL2.OR.I.GT.NRR)GO TO 232
      COUNTS=COUNTS+YC(I)
      232 CONTINUE
      AREA=2.50663*(CO*SIGMAO+DO*SIGMAO)
      CHISQ=0.0
      DO 275 I=NPL,NPR
      NPGSS=NPR-NPL+1
      IF(CO.LT.5.0)GO TO 86
      IF(DO.LT.5.0)GO TO 86
      VAR=(YC(I)-PX(I))**2
      VAR2=SQRT(VAR)
      VARI=VARI+VAR
      STU=2.0
      STU2=SQRT(STU)
      DENOM1=(CO**2+DO**2)/(STU2*(CO+DO))
      DENOM2=EXP(-(XMU1-XMU2)**2/(4.0*SIGMAO**2))
      DENOM3=DENOM1+((STU2*CO*DO)/(CO+DO))*DENOM2
      SET=VAR2/(NPGSS*DENOM3)
      CHISQ=CHISQ+SET
      IF(CHISQ.GT.10.0)GO TO 86
      275 CONTINUE
     *
      86 PRINT 800
      800 FORMAT(//3X,*FWHM*,4X,*CHISQ/VARI*,7X,*MU1/MU2*,5X,
     +*CO/DO*,9X,*COUNTS/AREA*)
      PRINT 810,FWHM,CHISQ,XMU1,CO,COUNTS
      810 FORMAT(/2X,F7.3,F13.8,3F13.3)
      PRINT 820,VARI,XMU2,DO,AREA
      820 FORMAT(10X,E12.6,2X,3F13.3)
      PRINT 821
      821 FORMAT(//2X*CH.#*5X,*Y(I)*8X,*PX(I)*10X,*DY(I)*10X,
     +* YC(I)*)
      PRINT 822,(X(I),Y(I),PU(I),DPU(I),YC(I),I=NPL,NPR)
      822 FORMAT(F4.0,F10.0,3F15.3)
      END
      SUBROUTINE GSS
      DIMENSION P(12),A(6,6),B(6),C(6),X(2048),Y(2048),PL(12),
     +PR(12),BL(12),BR(12)
      COMMON/1/X,Y,M,NUMBER,NL1,NL2,NR1,NR2,B,C,A
      EQUIVALENCE (PL,BL),(PR,BR)
      IF(M.EQ.5)GO TO 100
      IF(M.EQ.3)GO TO 10
     *
      10 M2=M*2
      DO 13 I=1,M2
      PL(I)=0.0
      DO 11 J=NL1,NL2
      11 PL(I)=PL(I)+X(J)**I
      PR(I)=0.0
      DO 12 K=NR1,NR2
      12 PR(I)=PR(I)+X(K)**I
      13 P(I)=PL(I)+PR(I)
```

```
S;53-L;53
      *
       N=M+1
       DO 30 I=1,N
       DO 30 J=1,N
       K=I+J-2
       IF(K)29,29,28
       28 A(I,J)=P(K)
       GO TO 30
       29 A(I,1)=NUMBER
       30 CONTINUE
      *
       BL(1)=0.0
       DO 21 J=NL1,NL2
       21 BL(1)=BL(1)+Y(J)
       BR(1)=0.0
       DO 22 J=NR1,NR2
       22 BR(1)=BR(1)+Y(J)
       B(1)=BL(1)+BR(1)
      *
       DO 25 I=2,N
       BL(I)=0.0
       DO 23 J=NL1,NL2
       23 BL(I)=BL(I)+Y(J)*(X(J)**(I-1))
       BR(I)=0.0
       DO 24 J=NR1,NR2
       24 BR(I)=BR(I)+Y(J)*(X(J)**(I-1))
       25 B(I)=BL(I)+BR(I)
       NM1=M
       GO TO 101
      *
       100 N=M
       NM1=M-1
       101 DO 300 K=1,NM1
       KP1=K+1
       L=K
       DO 400 I=KP1,N
       IF(ABSF(A(I,K))-ABSF(A(L,K)))400,400,401
       401 L=I
       400 CONTINUE
       IF(L-K)500,500,405
       405 DO 410 J=K,N
       TEMP=A(K,J)
       A(K,J)=A(L,J)
       410 A(L,J)=TEMP
       TEMP=B(K)
       B(K)=B(L)
       B(L)=TEMP
       500 DO 300 I=KP1,N
       FACTOR=A(I,K)/A(K,K)
       A(I,K)=0.0
       DO 301 J=KP1,N
       301 A(I,J)=A(I,J)-FACTOR*A(K,J)
       300 B(I)=B(I)-FACTOR*B(K)
```

```
L;20
      C(N)=B(N)/A(N,N)
     *
      I=NM1
      710 IP1=I+1
      SUM=0.0
      DO 700 J=IP1,N
      700 SUM=SUM+A(I,J)*C(J)
      C(I)=(B(I)-SUM)/A(I,I)
      I=I-1
      IF(I)900,900,710
     *
      900 IF(M.EQ.3)GO TO 930
      RETURN
      930 PRINT 726
      726 FORMAT(//*THE BACKGROUND EQUATION IS :*)
      PRINT 950,C(1),C(2),C(3),C(4)
      950 FORMAT(*Y = *,E11.3,*+*,E11.3,*X +*,E11.3,*X^2 +*,E11.3,
     +*X^3*)
      RETURN
      END
```

BIBLIOGRAPHY

1 P. G. Hoel, Introduction to Mathematical Statistics, (John Wiley & Sons 1966)

2 Robley D. Evans, Methods of Experimental Physics: Vol. 5 Part B, Nuclear Physics, (Academic Press 1963)

3 W. R. French et al., Am. J. Phys. Vol. 37 No. 1 Jan.69

4 A. Melissinos, Experiments in Modern Physics, (Academic Press 1967)

5 C. M. Davisson and R. D. Evans, Rev. Mod. Phys. 24, 107 (1952)

6 Paul Quittner, Gamma-Ray Spectroscopy, (Adam Hilger LTD. 1972)

7 R. L. Heath, R. G. Hermel et al., Nucl. Instr. & Meth. 57 (1967) 46

8 L. Varnell and J. Trischuck, Nucl. Instr. & Meth. 76 (1969) 109

9 U. U. Anders, Nucl. Instr. & Meth. 68 (1969) 205

10 M. A. Mariscotti, Nucl. Instr. & Meth. 50 (1967) 309

11 Herbert P. Yule, Anal. Chem. 40 (1968) 1480

12 D. P. Donnelly, M. L. Wiedenbeck, Nucl. Instr. & Meth. 64 (1968) 26

13 Paul Quittner, Nucl. Instr. & Meth. 76 (1969) 125

14 James B. Scarborough, Numerical Mathematical Analysis, (John Hopkins Press 1966)

15 I. S. Sokolnikof and R. M. Redheffer, Mathematics of Modern Physics and Engineering, (Mc Graw-Hill 1966)

16 P. W. Williams, Numerical Computation, (Nelson, London 1972)

17 G. Wallace and G. E. Coote, Nucl. Instr. & Meth. 74 (1969) 353

18 Nuclear Data Tables A8. 1970

19 G. Aubin, S. Monaro et al. , Nucl. Instr. & Meth. 76 (1969) 93

20 Kai M. B. Siegbahn, Alpha-Beta & Gamma Spectroscopy, (North-Holland, Amsterdam 1965)

21 Table of Isotopes, 6th Edition, C. M. Lederer, J. M. Hollander I. Perlman

22 K. A. Gromow, B. M. Sabirov et al. , Phys. Ser. 33 (1969)1510

23 R. S. Mowatt, Can. J. Phys. 48 (1970) 2606

24 D. H. White et al. , Nucl. Instr. & Meth. 77 (1970) 261

25 Atomic Data and Nuclear Data Tables, Vol. 13 Feb. 1974

26 E. M. Pugh and G. H. Winslow, The Analysis of Physical Measurements, (Addison-Wesley 1966)

27 J. R. Harvey, Nucl. Instr. & Meth. 86 (1970) 189

28 J. M. Freeman, J. G. Jenkin, Nucl. Instr. & Meth. 43 (1966) 269

29 H. Seyfarth et al. , Nucl. Instr. & Meth. 105 (1972) 301